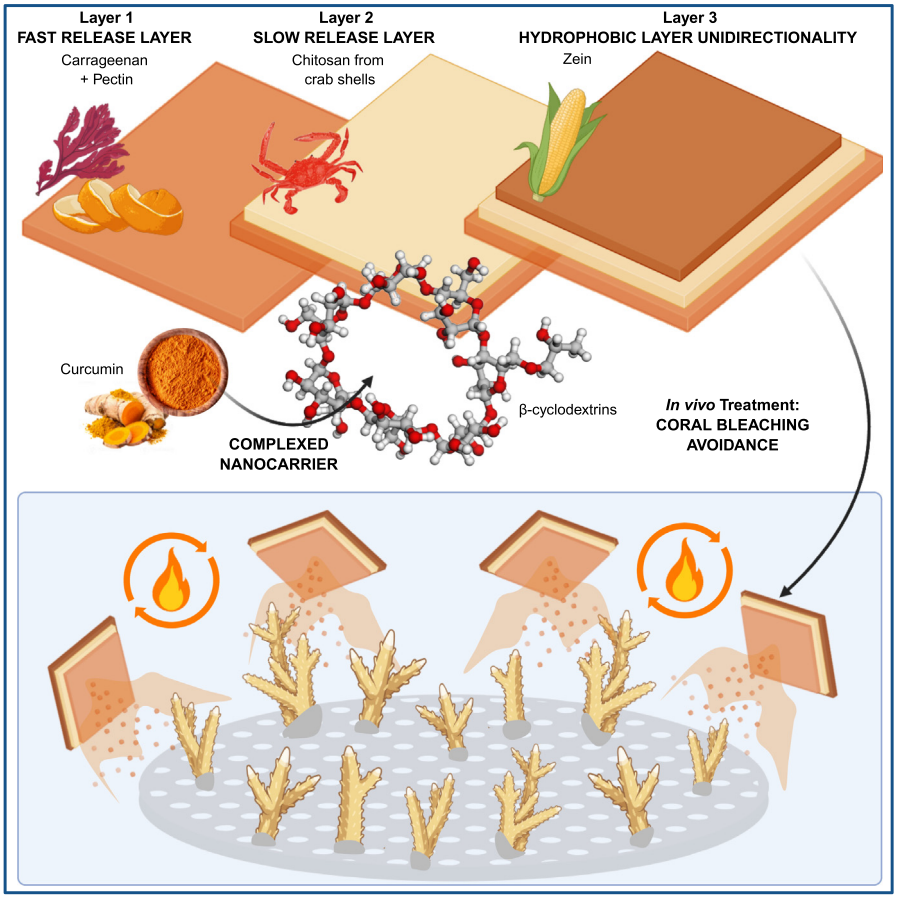
CellPress OPEN ACCESS

Trends in Biotechnology

Research Article

Tunable underwater curcumin release through a three-layered film system to mitigate oxidative stress in corals



A biobased multilayered film system for controlled curcumin release has been designed to mitigate oxidative stress in corals. Without direct contact, the system preserves chlorophyll content and Symbiodiniaceae density in corals exposed to rising temperatures, providing a sustainable strategy to enhance coral resilience under thermal stress events.

Camilla Rinaldi, Marco Contardi, Valerio Isa, Gabriele Corigliano, Lorenzo Ravelli, Vincenzo Scribano, Martina Facchinelli, Elena Bellini, Enrico Montalbetti, Davide Seveso, Silvia Lavorano, Paolo Galli, Simone Montano, Athanassia Athanassiou

camilla.rinaldi@iit.it (C. Rinaldi),
marco.contardi@unimib.it
(M. Contardi),
simone.montano@unimib.it
(S. Montano)
athanassia.athanassiou@iit.it
(A. Athanassiou).

Highlights

We developed a biobased underwater multilayered film system for controlled drug delivery to corals.

Without requiring direct contact, the system effectively reduced oxidative stress in corals exposed to increasing temperatures.

Ensuring a sustained, controlled, unidirectional release of curcumin, the film maintained high levels of chlorophylls, preserved Symbiodiniaceae density, and minimized lipid peroxidation, advancing antioxidant-based reef conservation strategies.

The technology has been designed with biodegradable, eco-friendly, and low-cost materials through industrially relevant techniques.

The presented platform reached a level of development corresponding to technology readiness levels 4–5.

Trends in Biotechnology, Month 2026, Vol. xx, No. xx
https://doi.org/10.1016/j.tibtech.2026.09.012

© 2026 The Author(s). Published by Elsevier Ltd. This is an open access article under the CC BY license (http://creativecommons.org/licenses/by/4.0/).

Trends in Biotechnology

CellPress OPEN ACCESS

Research Article

Tunable underwater curcumin release through a three-layered film system to mitigate oxidative stress in corals

Camilla Rinaldi [1,2,*], Marco Contardi [2,*], Valerio Isa [2,3], Gabriele Corigliano [1,2], Lorenzo Ravelli [1,2], Vincenzo Scribano [1,2], Martina Facchinelli [1,2], Elena Bellini [1,2], Enrico Montalbetti [2,3,4], Davide Seveso [2,3,4], Silvia Lavorano [5], Paolo Galli [2,3,4], Simone Montano [2,3,4,*,#], and Athanassia Athanassiou [1,*,#]

Coral bleaching, primarily driven by thermal stress and oxidative damage, threatens reef ecosystems worldwide. In this article, an eco-friendly, biocompatible, three-layered film system for controlled underwater delivery of curcumin directly to corals is proposed. This multilayered structure enables tunable, continuous, and directional drug release through a curcumin–β-cyclodextrin-complexed nanocarrier. Morphological, chemical, and mechanical analyses confirmed the system's structural integrity, water-absorption capacity, and hydrogel-like behavior, making it suitable for underwater applications. *In vivo* tests on *Stylophora pistillata* under a four-phase bleaching setup showed that, even without direct contact, the film may contribute to mitigating oxidative stress in corals, as evidenced by higher chlorophyll content, greater Symbiodiniaceae density, and reduced lipid peroxidation compared with untreated stressed corals. Overall, these results indicate a technology maturity corresponding to a technology readiness levels of 4–5 and demonstrate the potential of underwater drug delivery platforms for controlled and sustained release of antioxidants to mitigate oxidative stress in corals and, potentially, other marine species.

Introduction

Coral reefs are among the planet's most vital biodiversity hotspots, supporting millions of people through fisheries, coastal protection, and tourism, representing an ecological asset valued at US $10 trillion [1–3]. Despite their ecological and socioeconomic importance, these ecosystems have experienced substantial declines over the past decades, largely driven by anthropogenic stressors including overfishing, pollution, and climate change [4–8]. Rising sea temperatures and increasing CO_2 levels have been identified as key factors accelerating the loss of coral reefs [9,10], directly triggering coral bleaching and disease outbreaks [11]. Prolonged thermal stress disrupts the symbiosis between reef-building corals and their Symbiodiniaceae, leading to algal expulsion and host cell apoptosis [12,13]. Apart from heat stress, other potential causes that can trigger bleaching are excessive exposure to light, cold, hypoxia, high nitrate, and high ammonia concentrations. Prolonged exposure to these stressors can activate different biomolecular cascades within coral cells, leading to symbiosis breakdown. The most widely accepted explanations are the oxidative stress and carbon limitation hypotheses, which may also act in combination. In all cases, the outcome is an overproduction of **reactive oxygen and nitrogen species (ROS and RNS)** (see Glossary), which damage DNA, proteins, and lipids within cells, ultimately causing coral dysbiosis and bleaching [14–16].

Technology readiness

The underwater three-layered film system presented here was designed for coral bleaching mitigation by reducing oxidative stress through the controlled, continuous, and unidirectional release of a curcumin–β-cyclodextrin complexed nanocarrier. Following extensive *in vitro* and *in vivo* characterization, the platform has been evaluated at technology readiness levels (TRLs) 4–5. The antioxidant capacity of the system was successfully assessed both under laboratory conditions and at Genoa Aquarium, where it demonstrated effectiveness in mitigating coral bleaching damage when applied on *Stylophora pistillata* nubbins exposed to increasing temperatures. Material characterization suggested the potential applicability of the system across different coral morphologies and under real reef conditions, supported by preliminary field observations in the Maldives.

To progress toward higher TRLs, the next steps should focus on translating the current proof of concept into a reproducible and scalable field-deployment strategy. In natural reef environments, key challenges include optimizing the anchoring of the material to different coral morphologies and environmental conditions, determining who should position the material *in situ*, identifying the most appropriate locations and number of units to be deployed, and assessing overall effectiveness across large-scale reef areas. The development of standardized deployment protocols, potentially supported by trained robotic systems, could facilitate consistent application

© 2026 The Author(s). Published by Elsevier Ltd. This is an open access article under the CC BY license (http://creativecommons.org/licenses/by/4.0/).

Numerous actions have been taken worldwide to tackle and mitigate coral reef degradation, ranging from governance measures to reduce local stressors to experimental restoration techniques [17]. Restoration efforts, defined as interventions aimed at actively assisting ecosystems' recovery [18], are key strategies to combat the dramatic decline of coral cover worldwide [19]. Nevertheless, most approaches remain largely in early-stage trials with limited evidence of long-term success in natural reefs. Examples include underwater nurseries and reef stars (spiders); innovative tools such as 3D-printed hydrogels for Symbiodiniaceae cultivation [20]; clay-based substrates [21]; bio-based coral putties for coral anchoring in both aquaria and natural reefs [22–24]; and experimental microbial-based therapies [25]. While some strategies have shown promising preliminary outcomes under controlled conditions, their large-scale efficacy and ecological safety in natural reef environments remain uncertain.

Among emerging mitigation strategies, targeted antioxidant delivery has gained interest due to its potential to scavenge bleaching-induced ROS in coral tissue. Previous studies have explored antioxidant delivery using different approaches. Roger and colleagues [26] administered antioxidant nanoceria particles to free-living Symbiodiniaceae, providing early evidence of the potential of antioxidant-based interventions. Contardi and colleagues [27] developed a first prototype of a material for underwater, controlled delivery of the natural antioxidant curcumin to corals, introducing the delivery of active agents in close proximity to target marine organisms. While these pioneering studies showed some efficacy under thermal stress, they also revealed limitations such as uncontrolled dispersion, limited targeting, and the need for optimized material design and drug release control. To overcome these challenges, we developed a **three-layered film system** for underwater, directional, and sustained delivery of curcumin, a natural antioxidant derived from the *Curcuma longa* plant. Each layer was engineered for a specific function through its polymeric composition: a carrageenan–pectin first layer for initial burst release, a chitosan-based second layer as a drug reservoir enabling slower release, and an outer zein protein shield layer for unidirectional delivery and enhanced resistance of the system to degradation in water. These natural, biodegradable polymers, sourced from seaweed and citrus peel [28,29], crab shells [30], and maize [31], respectively, ensure environmental compatibility. Because of curcumin's low solubility in water, it was encapsulated in 2-hydroxypropyl-β-cyclodextrins, cyclic oligosaccharides with a hydrophobic cavity and hydrophilic exterior, to form a nanocarrier complex (**cur-β-CD nanocomplex**) that was integrated into the first two layers to improve dispersion and release [32,33]. The system was thoroughly characterized in terms of physicochemical properties, release kinetics, water resistance, and coral biocompatibility. Its efficacy was tested through *in vitro* and *in vivo* assays using a 30-day thermal bleaching setup on a model species (*Stylophora pistillata*) in aquaria. Results suggested that the cur-β-CD-loaded system may significantly mitigate bleaching effects, preserving coral morphology, chlorophyll content, Symbiodiniaceae density, and reduce oxidative stress markers such as superoxide dismutase (SOD), catalase (CAT), glutathione S-transferase (GST), glutathione reductase (GR), and lipid peroxidation (LPO).

Although further studies are required to assess its large-scale production and efficacy in natural coral reef environments [technology readiness levels (TRLs) 6–7], the designed three-layered film system has progressed from a general conceptual formulation to fabrication using relevant industrial processing techniques and experimental validation in an *in vivo* coral model (medium TRLs 4–5). These achievements highlight the potential of this technology as a biodegradable and eco-friendly platform for enhancing coral resilience to thermal stress through the controlled release of antioxidant molecules.

over large reef areas. In parallel, optimizing the fabrication process from laboratory-scale procedures to continuous industrial production represents another key point, which can be achieved by adapting the proposed formulation to the corresponding industrial version of the machinery. Addressing these technological and field-deployment challenges will provide the basis for advancing this three-layered film system toward higher TRLs and, ultimately, toward controlled, scalable production and safe applications in case of massive coral bleaching events.

[1]Smart Materials, Istituto Italiano di Tecnologia, Genova, Italy
[2]Department of Earth and Environmental Sciences (DISAT), University of Milano-Bicocca, Milan, Italy
[3]MaRHE Center (Marine Research and High Education Center), Magoodhoo Island, Faafu Atoll, Maldives
[4]NBFC (National Biodiversity Future Center), 90133 Palermo, Italy
[5]Costa Edutainment SpA – Acquario di Genova, Genova, Italy
[#]These authors are co-last authors

*Correspondence:
camilla.rinaldi@iit.it (C. Rinaldi),
marco.contardi@unimib.it (M. Contardi),
simone.montano@unimib.it
(S. Montano), and
athanassia.athanassiou@iit.it
(A. Athanassiou).

CellPress
OPEN ACCESS

Results

Characterization of films

Morphological analysis. A schematic representation of the film's three-layer preparation, along with photographs of each layer, is shown in Figure S1 in the Supplemental information online. The first layer, composed of carrageenan, pectin, and PVP, loaded with Cur-β-CD and fabricated using the **solvent casting** method, exhibits a reddish color, as shown in Figure S1A. In Figure S1B, the preparation of the second layer, composed of chitosan and PVP, loaded with Cur-β-CD, and deposited on the first layer by the **rod coating** method, is shown. Finally, the third layer was obtained via the **spray coating** method by spraying a zein solution onto the bilayer (Figure S1C). For the sake of clarity, a terminology legend is provided in the 'Supplemental information' section.

SEM images of the surface of the monolayer, bilayer, and three-layer systems were acquired to study the morphology of the samples (Figure 1A–C). The first layer showed a relatively rough surface, while the second and third layers presented a smoother surface, most likely due to their different preparation methods. Figure 1D–F shows cross-section images of the respective samples. The separation between the two layers of the bilayer was only slightly evident because of their similar polymeric composition, mostly based on PVP and polysaccharides, and is indicated by the orange dashed line in Figure 1E. The cross-section of the three-layer system (Figure 1F) shows the different morphology of the third layer relative to the other two due to a composition based on zein protein. The separation between layers 1 and 2 is highlighted in orange, while the blue line indicates the interface between the bilayer and the third layer. The thickness of the different layers was calculated by comparison of the total thickness of the monolayer (≈180 ± 10 μm), the bilayer (≈280 ± 20 μm), and the three-layer (≈330 ± 35 μm) systems, indicating that the thicknesses of the second and third layers were ≈100 ± 10 μm and ≈50 ± 15 μm, respectively. Thickness was evaluated using ImageJ software combined with measurements obtained using a digital caliper, and the results for all the samples are reported in Table S1 in the Supplemental information online.

Finally, SEM-EDX (Scanning Electron Microscopy – Energy Dispersive X-ray spectroscopy) analysis was performed on the bilayer system to further distinguish the first two layers by tracing sulfur (S) and other elements present only in carrageenan and thus in the first layer. Indeed, sulfur was observed in the first layer as the main element (Figure S2 in the Supplemental information online), whereas the second layer did not show a significant presence of this element and was mostly composed of carbon.

Chemical and mechanical characterization. The UV–Vis (Ultraviolet-Visible Spectroscopy) absorbance of pristine curcumin and cur-β-CD in a water–ethanol mixture was measured to evaluate the inclusion of the antioxidant compound within the ring-shaped molecules prior to film production. A shift in the main curcumin absorption band was observed from 425 nm for pristine curcumin to 434 nm for the cur-β-CD system (Figure 2A). This red shift, together with increased water solubility of the cur-β-CD system, suggests successful incorporation of curcumin and the resulting formation of a complexed nanocarrier, as reported in the literature [34,35].

The fabricated monolayer, bilayer, and three-layer systems, and their pristine components, were chemically characterized by ATR-FTIR to investigate the chemical nature of the layers and possible interactions among their ingredients. Spectra are reported in Figure 2B and Figures S3 and S4 in the Supplemental information online. In Figure S3A, the spectra of the first-layer components are reported, and their characteristic peaks are assigned. The spectrum of carrageenan (black line) shows the characteristic O–H stretching between 3400 and 3100 cm^{-1}, absorption bands between 1350 and 1200 cm^{-1} corresponding to asymmetric stretching of the O═S═O and

Glossary

Cur-β-CD nanocomplex: the complex formed by the encapsulation of curcumin within the hydrophobic cavity of β-cyclodextrin. This complexation enhances the aqueous solubility and bioavailability of curcumin upon administration.

Reactive oxygen and nitrogen species (ROS and RNS): reactive molecules whose production can increase under oxidative and nitrosative stress. In the context of coral bleaching, elevated ROS and RNS levels contribute to cellular damage and coral physiological dysfunction, potentially promoting the breakdown of the coral–Symbiodiniaceae symbiosis and the subsequent expulsion of Symbiodiniaceae.

Rod coating: a technique used at both laboratory and industrial scales to deposit a thin and uniform layer of liquid material onto a flat substrate. In this case, the method is used to deposit the second layer of the film system onto the first layer.

Solvent casting: a simple technique for producing uniform polymer films by dissolving a polymer in a suitable solvent, casting the resulting solution into a mold, typically made of PDMS (polydimethylsiloxane), and allowing the solvent to evaporate. In this case, the method is used to produce the first layer of the film system.

Spray coating: a method for applying a thin and uniform layer of liquid onto a surface by atomizing the material into fine droplets using a spray gun. This technique enables the rapid application of the material both onto the surface of an underlying layer and its sides. In this case, the method is used to apply the third, hydrophobic zein layer of the system onto the previously developed first and second layers.

Three-layered film system: the final multilayer material obtained by sequentially depositing three layers using different coating techniques—solvent casting for layer 1, rod coating for layer 2, and spray coating for layer 3. This three-layered film system enables the unidirectional and sustained release of antioxidant compounds, which are essential for coral bleaching treatment.

Transwell system: a well-plate-based system in which each well is divided into two separate compartments by a porous membrane, enabling the study of cell migration, growth, and interactions.

S═O groups, and strong, broad absorption bands in the 1100–1000 cm^{-1} region, which represent C–O–C and C–O stretching typical of polysaccharides [36]. In the pectin spectrum (red line), the O–H stretching mode appears between 3500 and 3100 cm^{-1}, and the two strong bands at 1734 and 1607 cm^{-1} indicate the ester carbonyl (C═O) groups and the carboxylate ion stretching band (COO–), respectively [37]. The main bands of PVP (blue line) were associated with asymmetric and symmetric CH_2 stretching modes at 2951 cm^{-1} and 2868 cm^{-1}, respectively, and the C═O stretching mode at 1657 cm^{-1} [38]. The spectrum of curcumin (green line) showed free O–H stretching vibration at 3509 cm^{-1}, C–H aromatic and aliphatic stretching vibration from 3071 to 2845 cm^{-1}, C═O and C═C stretching vibration of the inter-ring chain at 1628 cm^{-1}, C═O stretching vibration at 1506 cm^{-1}, CH_3 in-plane bending vibration of the methoxy group at 1457 cm^{-1}, C–O–H in-plane bending vibration connected to the enolic form at 1232 cm^{-1}, O–CH_3 stretching vibration of the aromatic ring connected to the enolic part at 1111 cm^{-1}, and C–O–C stretching vibration of the aromatic ring connected with the enolic part at 1022 cm^{-1} [39]. Finally, the purple line reported the characteristic peaks of 2-hydroxypropyl-β-cyclodextrin at 3368 cm^{-1} and 2926 cm^{-1}, corresponding to O–H and C–H stretching vibration, respectively, at 1420 cm^{-1} and 1369 cm^{-1}, corresponding to O–H and C–H bending vibration, respectively, and at 1158 cm^{-1} corresponding to C–O–C glycosidic stretching vibration. In the end, C–C and C–O stretching vibrations gave peaks at 1076 cm^{-1} and 1020 cm^{-1}, respectively. From 945 to 606 cm^{-1}, stretching corresponding to the cyclodextrin ring was highlighted [40]. The spectrum of the monolayer (purple line in Figure S3A) showed bands mostly associated with the polymeric components. In the carbonyl stretching region, some variations were observed. The C═O of PVP had a red shift from 1657 to 1647 cm^{-1}. Under this band, the ester carbonyl (C═O) group of pectin is also present, which moved from 1734 to around

In this case, a piece of the material was placed on the porous membrane to investigate the directional release of curcumin. The results demonstrated that approximately 80% of the curcumin was released in one direction, indicating predominantly unidirectional drug release.

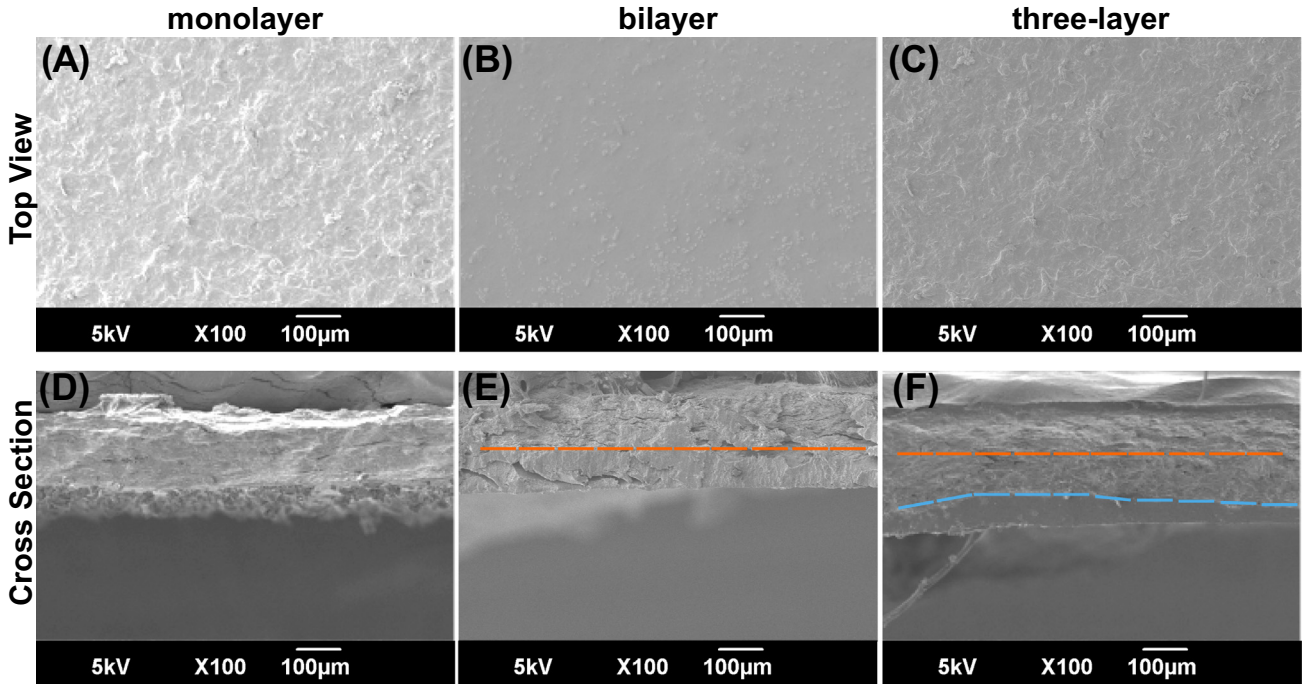


Figure 1. Morphological characterization of the three-layered film system. Top-view SEM images of (A) the monolayer showing the surface of the first layer, (B) the bilayer showing the surface of the second layer, and (C) the three-layered sample showing the surface of the third layer. Cross-sectional SEM images of (D) the monolayer, (E) the bilayer, and (F) the three-layered sample. Orange and blue dashed lines indicate the separations between the first and second layers and between the second and third layers, respectively. SEM: scanning electron microscopy.

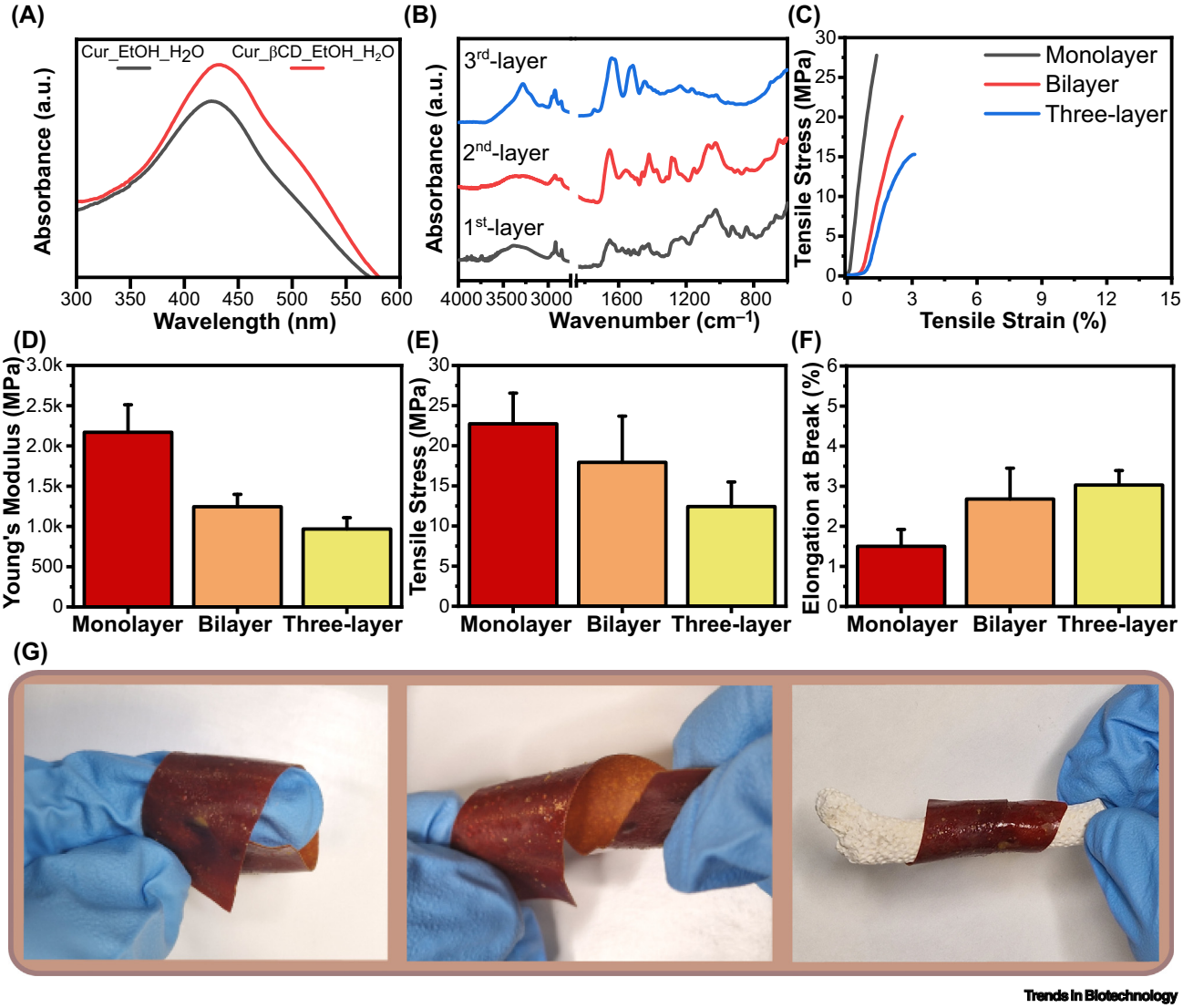


Figure 2. Chemical and mechanical characterization of the three-layered film system. (A) UV–Vis absorbance of pristine curcumin and of curcumin complexed within the nanocarrier β-CD in an ethanol–water solution. (B) FT-IR normalized spectra for the upper part of the monolayer, the bilayer (layer 2 up), and the three-layered film system (layer 3 up). (C) Stress–strain curves for the monolayer, bilayer, and three-layered film system. (D) Young's modulus; (E) tensile stress at maximum load; and (F) elongation at break for all systems. The results are expressed as the mean and standard deviation, with $n = 10$. (G) Photographs of the three-layered material folded and wrapped around fingers and a coral skeleton. β-CD: β-cyclodextrin; FT-IR: Fourier transform infrared; Uv-Vis: Ultraviolet-Visible Spectroscopy.

1647 cm^{-1}, overlapping with the C═O of PVP. Similarly, the carboxylate group shifted from 1607 to 1601 cm^{-1} in the monolayer spectrum. These red shifts are typically attributed to the formation of hydrogen bonds (H-bonds) among the polymeric chains of the matrix.

FTIR spectra corresponding to the upper part of the bilayer system, thus to the second layer and its components, are reported in Figure S3B. PVP, curcumin, and β-cyclodextrins exhibit the same spectra as previously described in the monolayer and are shown here as black, blue, and green lines, respectively. Moreover, the peaks of chitosan are highlighted in red. The region between 3360 and 3290 cm^{-1} corresponds to N–H and O–H stretching, while the absorption bands

around 2900 cm^{-1} can be attributed to asymmetric and symmetric C–H stretching. The stretching of C═O (Amide I) occurs at 1649 cm^{-1}, the Amide II at 1582 cm^{-1}, and the stretching of C–N (Amide III) at 1319 cm^{-1}. Lastly, the absorption band at 1153 cm^{-1} can be attributed to the stretching of the C–O–C bridge, and the bands at 1057 and 1024 cm^{-1} to C–O stretching [41]. The purple line represents the FTIR spectrum of the second layer of the material. Peaks assigned to PVP, chitosan, and curcumin can be recognized. The main shifts can be found in the merged peaks of the C═O band of PVP and the Amide I that fall at 1645 cm^{-1} instead of 1657 cm^{-1} and 1649 cm^{-1}, respectively.

Finally, the peaks of zein powder and the third layer, corresponding to the upper part of the three-layer system, are shown in Figure S3C. The zein spectrum is shown in black, while the complete spectrum of the third layer is in red. The two main peaks of zein powder were attributed to N–H and O–H at 3292 cm^{-1} and 3188 cm^{-1}, respectively; additional bands include aromatic and aliphatic C–H stretching between 3070 and 2853 cm^{-1} and Amide I at 1645 cm^{-1} [42]. In the third layer of the three-layer system, zein was solubilized and applied by spray coating. It shows the same peaks found in the powder, but it presents a shoulder in the Amide I peak, indicating an alteration of the secondary structure of the protein toward a higher presence of β-sheets and thus higher hydrophobicity [43–45].

Tensile tests for monolayer, bilayer, and three-layer samples were measured at 25°C and 44% relative humidity. Stress–strain curves for each system are shown in Figure 2C. The monolayer had a Young's modulus (YM) of ≈2170 MPa, the bilayer ≈1240 MPa, and the three-layer ≈970 MPa (Figure 2D). Tensile stress at maximum load (TSML) of ≈22 MPa, ≈18 MPa, and ≈12 MPa was found for the monolayer, bilayer, and three-layer films, respectively (Figure 2E). Finally, the elongation at break was ≈1.5%, ≈2.7%, and ≈3.0% in the monolayer, bilayer, and three-layer, respectively (Figure 2F). The initial monolayer proved to be robust, further stabilized by the H-bond interactions highlighted by the FTIR analysis. Adding the second layer produced a reduction of the YM and the TSML. This can be explained by the increased presence of PVP inside the overall composition of the material, which is a typically hygroscopic material, and its mechanical properties are commonly affected by humidity [27]. The three-layered film presented a further decrease in YM and TSML, making it slightly more flexible and ductile (photographs in Figure 2G). This is a crucial property, as it facilitates handling by operators and enables the material to conform to and wrap around corals of varying shapes. These variations in multilayered materials with respect to the individual components and unassembled layers have already been reported in the literature and have been explained as resulting from new polymeric rearrangements with interactions at the interfaces among the layers [46].

Film–water interaction and salinity-induced crosslinking

Films' interactions with Milli-Q (Manufacturer: Millipore Corporation) and seawater were investigated through swelling, gel fraction, and rheological analyses. The degree of swelling of monolayer, bilayer, and three-layered films immersed in Milli-Q water for 24 h is reported in Figure 3A. The monolayer system showed rapid swelling and consequent total dissolution after 40 min. The bilayer remained intact underwater for a few more hours, showing a peak swelling of ≈2000% at ≈1 h, with dissolution occurring in 4 h. Three-layered films, by contrast, were still recoverable after 24 h; they reached a swelling peak of ≈2500% after ≈3 h, after which they began to dissolve, although they were still measurable after 24 h due to the presence of the thin zein layer, which did not dissolve over such a short time span.

When placed in seawater, the films exhibited different behavior, as shown in Figure 3B. All of the systems were relatively stable in seawater, showing their highest swelling values after 3 h, of

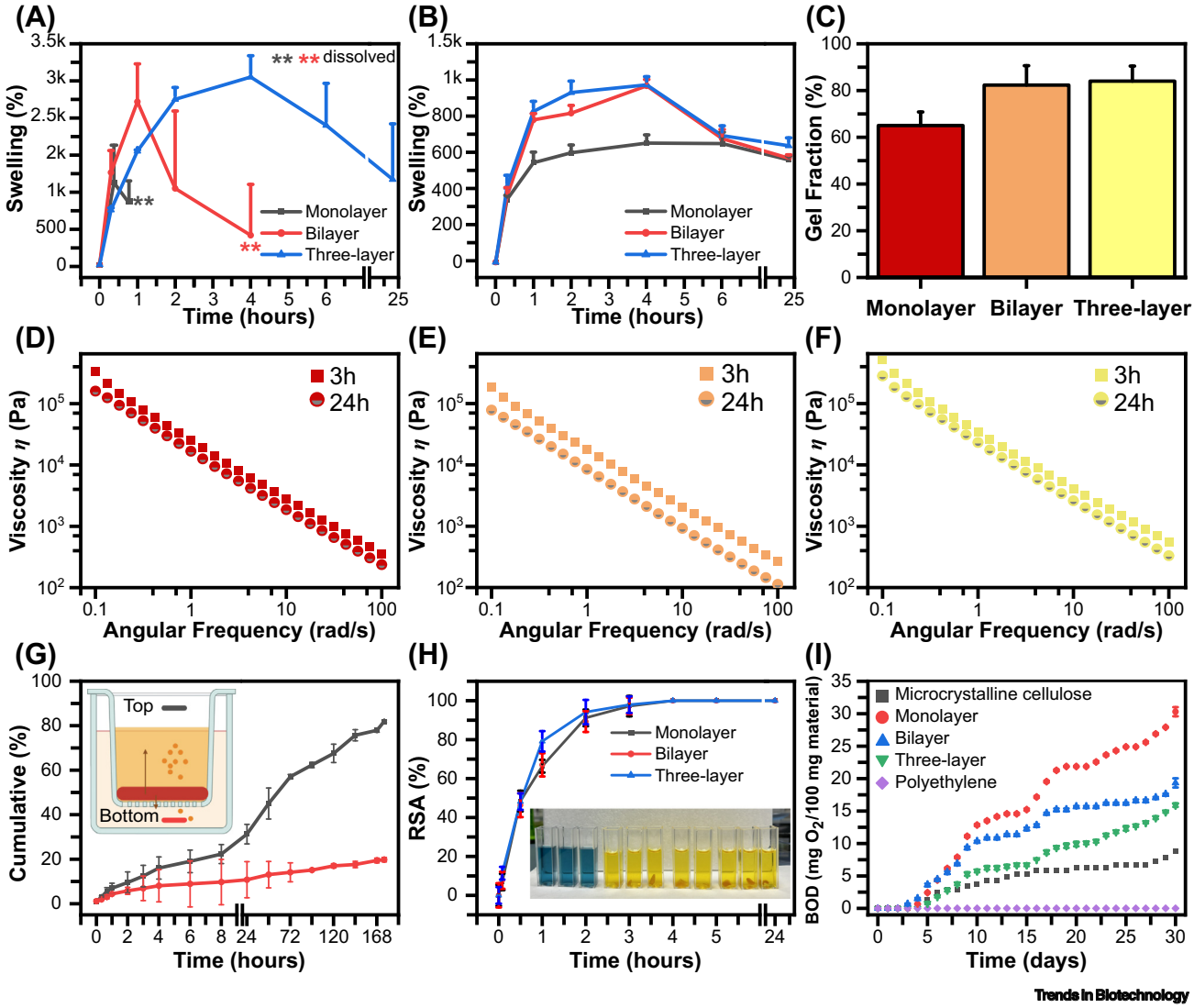


Figure 3. Film–water interaction, drug-release studies, antioxidant activity, and biodegradation properties. Swelling percentages of monolayer, bilayer, and three-layered film systems in (A) Milli-Q water and (B) seawater; (C) gel fraction results for monolayer, bilayer, and three-layered film systems after complete submersion in seawater. Results are shown as means and standard deviations with $n = 5$. Shear strain results from rheological tests on (D) monolayer, (E) bilayer, and (F) three-layered samples after 24 h submerged in seawater. (G) Data from the unidirectional, cumulative cur-β-CD release experiment from the three-layered system in a Transwell. The red line represents the bottom compartment of the Transwell, while the black one represents the upper compartment. The material is placed in the well with the zein-based hydrophobic layer in contact with the mesh membrane of the Transwell and the carrageenan-based hydrophilic layer toward the medium. (H) Radical scavenging activity of each system in the ABTS assay. A photograph of the cuvette with the control ABTS solution and the ABTS solution in contact with the materials after 24 h is shown. (I) BOD results for the monolayer, bilayer, and three-layered film systems compared with a positive control (microcrystalline cellulose) and a negative control (PE). Results are shown as means and standard deviations with $n = 3$. ABTS: 2,2′-azino-bis(3-ethylbenzothiazoline-6-sulfonic acid); BOD: biochemical oxygen demand; cur-β-CD: curcumin–β-cyclodextrin; PE: polyethylene; RSA: radical scavenging activity.

≈580% for the monolayer, ≈930% for the bilayer, and ≈960% for the three-layered system—and then stabilizing at around 500–600% after 24 h.

Figure 3C reports the gel fraction for each system in seawater, whereas, as mentioned before, this analysis could not be performed in Milli-Q water because the films dissolved. Gel fraction values were 65%, 80%, and 85% for the monolayer, bilayer, and three-layered systems,

respectively, after 24 h of immersion in seawater. To further highlight the stability of the materials in seawater, a photograph of the three-layered sample after 1 week of immersion is reported in Figure S5 in the Supplemental information online. In the image, the second (yellowish) and third (brownish) layers of the three-layered material are still easily recognizable, while the first layer dissolved.

Rheological analyses of the three systems upon immersion in seawater for 3 and 24 h were carried out to further characterize their physical state and mechanical properties. These two time points were chosen because the maximum degree of swelling was obtained after 3 h, and the swelling stabilized after 24 h (Figure 3B). Amplitude and frequency sweep tests were performed on the different samples.

The materials, both at 3 h and 24 h, exhibited gel-like behavior in hydrated conditions, as shown in Figure S6C,D in the Supplemental information online, in which all samples showed the elastic modulus (G') consistently higher than the viscous modulus (G'') across the entire frequency range. The three-layered system displayed the highest magnitudes of both G' and G'' at every time point.

Although they exhibited a solid, gel-like behavior, at 24 h all samples displayed a slight decrease in complex viscosity relative to 3 h, as shown in Figure 3D–F. This can be attributed to the increased water content after 24 h relative to the previous time point, confirming the swelling dynamics shown in Figure 3B. The results of the rheological analysis confirmed that, once immersed in seawater, the different layers are capable of absorbing and retaining seawater and of assuming a gel-like behavior, in agreement with what is expected for a hydrogel.

This different mode of interaction with Milli-Q water and seawater can be justified by the differences in ion concentration and pH between the two media. Indeed, the main polymers composing the films undergo chain crosslinking in the presence of ions. For instance, the presence of divalent ions, such as calcium ions (Ca^{2+}) found in seawater, has been widely shown to increase the water stability and mechanical properties of pectin [47–49]. Similarly, it is well known that carrageenan crosslinks in the presence of calcium ions (Ca^{2+}) and potassium ions (K^{+}), exhibiting hydrogel-like behavior [50–52]. Moreover, chitosan is much less soluble under basic conditions, further stabilizing the entire structure when immersed in seawater, which has a typical pH of 8.2 [53].

Drug release studies, antioxidant properties, and biodegradation properties

The three-layered material was designed to ensure a controlled, constant, and directional release of the cur-β-CD nanocomplex once immersed in seawater. Two experiments were carried out to evaluate the drug-release performance. The first examined the overall drug-release kinetics of the three layers under complete immersion in water and anisotropic conditions. The second investigated whether the protective, zein-based third layer could help direct the release in a specific direction.

Results for the diffusion of the cur-β-CD nanocomplex from all systems immersed in seawater are shown in Figure S7 in the Supplemental information online. The monolayer showed a burst-release profile, losing 80% of the drug within the first 4 h and reaching 100% in 24 h, which is consistent with the quick swelling behavior of this material. By contrast, for the bilayer and three-layered materials, the release occurred more slowly and was prolonged, reaching total drug release after 168 h. The release started almost immediately, reaching 30–40% after 8 h, which can be linked to drug diffusion from the first layer. After the initial burst of release, the

antioxidant compound was continuously released from the second layer in the bilayer and the three-layered samples. The reduced kinetics can be explained by the fact that the first layer did not dissolve after 24 h, as confirmed by the gel fraction results, and that the drug from the second layer needed to diffuse across this additional barrier. At the same time, contact with seawater markedly reduces the solubility of chitosan due to the slightly basic pH. Therefore, after the initial swelling within the first hours, the main driving force of the release can be attributed to the slow erosion of the first- and second-layer matrices, allowing an overall slow and constant diffusion of the drug.

To study the unidirectionality of cur-β-CD release, once the material was placed in close proximity to, or directly in contact with, the coral, a **Transwell system** was used, as shown in Figure 3G. The top represents the coral target, while the bottom simulates the marine environment. In the upper compartment, the release was constant and controlled, and after 24 h, approximately 30% of the cur-β-CD had diffused. At the same time, 10% of the overall dose was found in the lower compartment, which is probably due to the initial burst release and swelling of the film in the first hours of immersion. Subsequently, of the remaining dose, about 50% was released into the upper compartment, and the other 10% into the lower compartment. The qualitative difference in drug release is further illustrated in Figure S8 in the Supplemental information online, which shows aliquots collected at the 176 h withdrawal time point from the upper and lower compartments and placed in cuvettes. The aliquots exhibit a clear difference in color intensity. In summary, at the end of the experiment, 80% of the overall dose was found in the target compartment rather than the other side, demonstrating the excellent barrier properties of the hydrophobic third layer, allowing directional diffusion of the antioxidant toward the target organisms.

Since curcumin is well known for its antioxidant properties, ABTS assays were conducted to determine the antioxidant capacity of monolayer, bilayer, and three-layered film systems after fabrication. A three-layered film system without curcumin was also tested as a negative control. Results are reported in Figure 3H and Figure S9 in the Supplemental information online. After 4 h, all the tested samples showed the maximum percentage of radical scavenging activity, as is also evident from the absence of the typical ABTS blue color in the cuvette in the inset photo. The three-layered film without curcumin did not show any significant scavenging activity after 24 h, confirming that the antioxidant property of the technology is due to the presence of curcumin.

Finally, a fundamental point to verify is that the materials are biodegradable in that environment. For this reason, biochemical oxygen demand tests were conducted for monolayer, bilayer, and three-layered film systems. All samples were studied for 30 days. Microcrystalline cellulose was tested as a positive control for biodegradation, while polyethylene (PE) was tested as a negative control for biodegradation [54,55]. The main results are reported in Figure 3I. The monolayer showed the highest degradation rate, yielding a value of 30 mg O_2 per 100 mg of material. The bilayer showed an oxygen consumption of 20 mg O_2 per 100 mg, and the three-layered system 14 mg O_2 per 100 mg, still higher than the value of 10 mg O_2 per 100 mg obtained for microcrystalline cellulose. As expected, PE showed no signs of biodegradation.

Three-layered films on corals during an induced thermal stress model

The biocompatibility and efficacy of the three-layered film system in reducing thermal stress susceptibility were evaluated *in vivo* at the Genoa Aquarium using a four-phase coral bleaching setup with *S. pistillata*—a model species. An induced thermal stress model was designed to investigate the potential effect of the three-layered film system on corals under simulated

bleaching conditions. Specifically, four phases were reproduced: acclimation (A), heat stress (HS), bleaching (B), and recovery (R). Corals were divided into two different experimental groups: untreated controls and fragments treated with the three-layered film. The experimental setup of the coral bleaching experiment, with associated photographs of untreated and treated corals for each phase, is shown in Figure 4 and details are provided in Figure S10 in the Supplemental information online. For each phase, the temperature settings, duration, and number of corals sampled are reported.

Physiological parameters (chlorophyll content, Symbiodiniaceae density, and enzyme activity) were monitored to assess the overall health of the corals in the experiment. During the acclimation phase of 7 days at 25°C, schematically represented in Figure 4A, no significant morphological changes were observed between treated and untreated corals. The same was true for the heat stress phase (Figure 4B), during which the temperature progressively increased by 0.5°C per day, reaching 31°C after 12 days. However, after continuous exposure of the corals to 31°C for 1 week during the bleaching phase (Figure 4C), as well as at the end of the recovery phase, during which the temperature was gradually reduced by 1°C per day back to 25°C (Figure 4D), untreated corals exhibited small white spots, whereas treated corals appeared visually less affected, suggesting a possible protective effect of the three-layered film system.

To clarify the potential effect of the delivered cur-β-CD nanocomplex, bleaching biomarkers inside the coral tissue were analyzed at each phase for all experimental groups. All results are reported in Figure 5, and the different colors represent the different phases of the model. The bleaching phenomenon causes the breakdown of the symbiosis between the polyps and their algae; for this reason, as primary biomarkers, the content of chlorophyll *a*, chlorophyll c_2, and Symbiodiniaceae cell density were quantified. For these three biomarkers, no significant changes were noticed between the two experimental groups (treated and untreated) during the first two phases of the experiment (Figure 5A–C). However, during the bleaching phase, significant differences in the content of chlorophylls and Symbiodiniaceae cell density were observed between untreated control corals and those treated with the three-layered film system, with untreated corals showing consistently lower values. Specifically, chlorophyll *a* and c_2 levels were ~6.3 ± 0.1 μg/cm^2 and ~1.4 ± 0.2 μg/cm^2 in untreated corals, compared with ~8.1 ± 0.1 μg/cm^2 and ~2.1 ± 0.1 μg/cm^2 in treated corals, respectively [Chl_*a*: $^*P$ = 0.000077, effect size (η^2) = 0.977; Chl_c_2: $^*P$ = 0.013, η^2 = 0.834] (Figure 5A,B). Similarly, Symbiodiniaceae cell density was lower in untreated corals (~0.6 ± 0.1 × 10^6 cells/cm^2) than in treated ones (~1 ± 0.1 × 10^6 cells/cm^2) during the bleaching phase ($^*P$ = 0.00029, η^2 = 0.912). In the recovery phase, the trend was maintained despite no statistical significance being obtained for the two chlorophylls, whereas Symbiodiniaceae cell density was still significantly different, with values of ~0.7 ± 0.1 × 10^6 cells/cm^2 and ~1 ± 0.1 × 10^6 cells/cm^2 as shown in Figure 5C ($^*P$ = 0.0028, η^2 = 0.890).

One of the main causes of coral bleaching is oxidative stress, and corals, in response to this, produce enzymes that can buffer or scavenge the propagation of oxidative species. In this section, the levels of coral SOD, CAT, GST, and GR were evaluated, and the results are reported in Figure 5D–G, respectively. The overall activity level of these enzymes increased from the acclimation phase to the heat and bleaching phases because of the induced thermal stress. The level of SOD between the untreated and treated samples did not seem to differ strongly in trend during heat stress (≈0.81 U/mg), while it became slightly lower for the treated corals in the bleaching phase (untreated ≈ 0.87 U/mg, treated ≈ 0.72 U/mg). Instead, during the recovery phase, the treated corals presented a statistically much lower level of this enzyme (untreated ≈ 0.75 U/mg, treated ≈ 0.32 U/mg, $^*P$ = 0.0051, η^2 = 0.931). CAT was strongly expressed during the heat, bleaching, and recovery phases in the untreated corals with values of 0.058 K/mg, 0.054 K/mg,

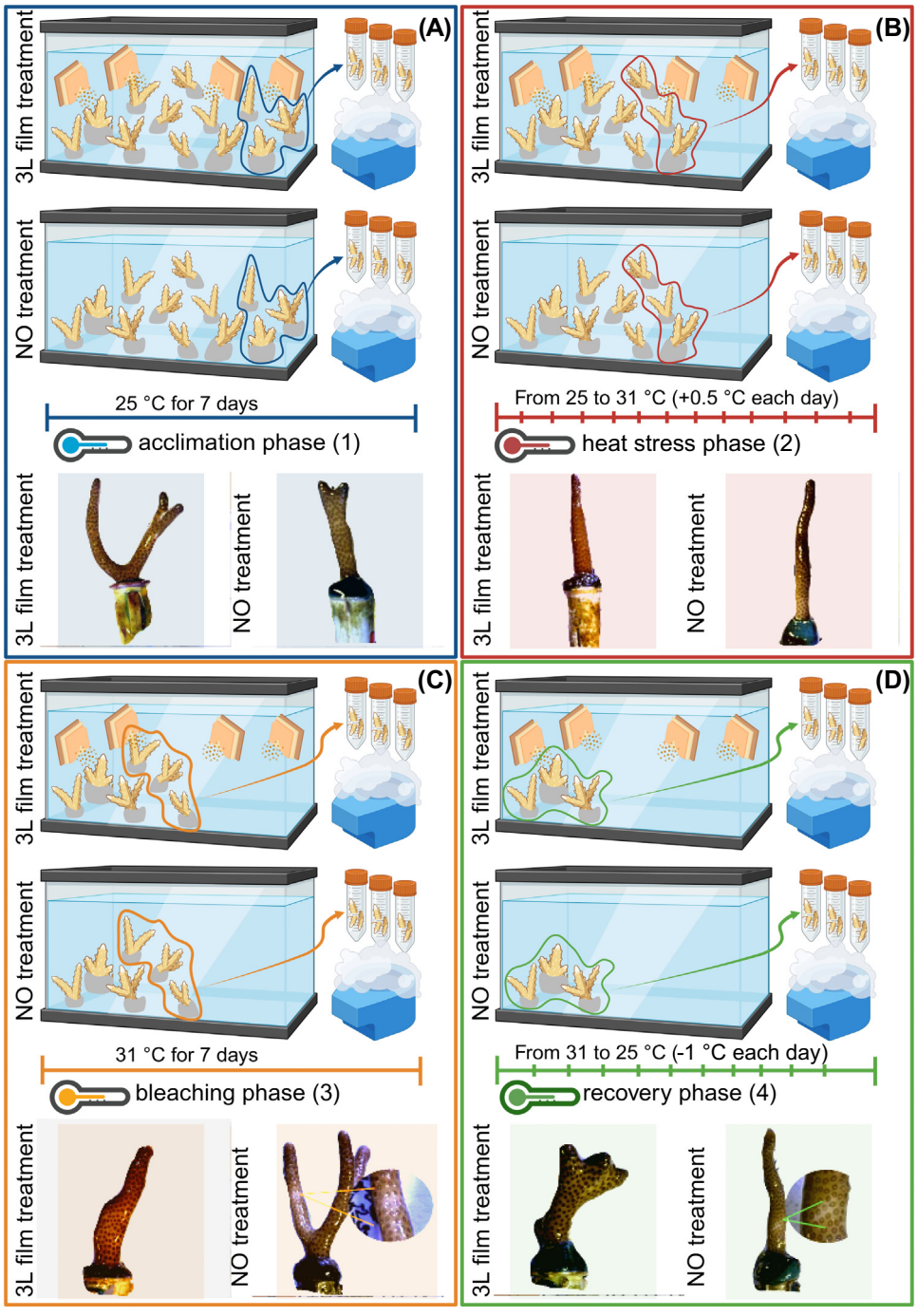


Figure 4. Schematic representation of each phase of the induced thermal stress experimental setup and corresponding visual results. At each phase [(A) acclimation, (B) heat stress, (C) bleaching, and (D) recovery] relevant comparisons between the untreated control corals and the corals treated with the three-layered film system were highlighted through qualitative images. Total number of corals: $n = 24$. Total number of corals in the control tank: $n = 12$. Total number of corals in the treatment tank: $n = 12$. Number of corals sampled after each phase: $n = 3$.

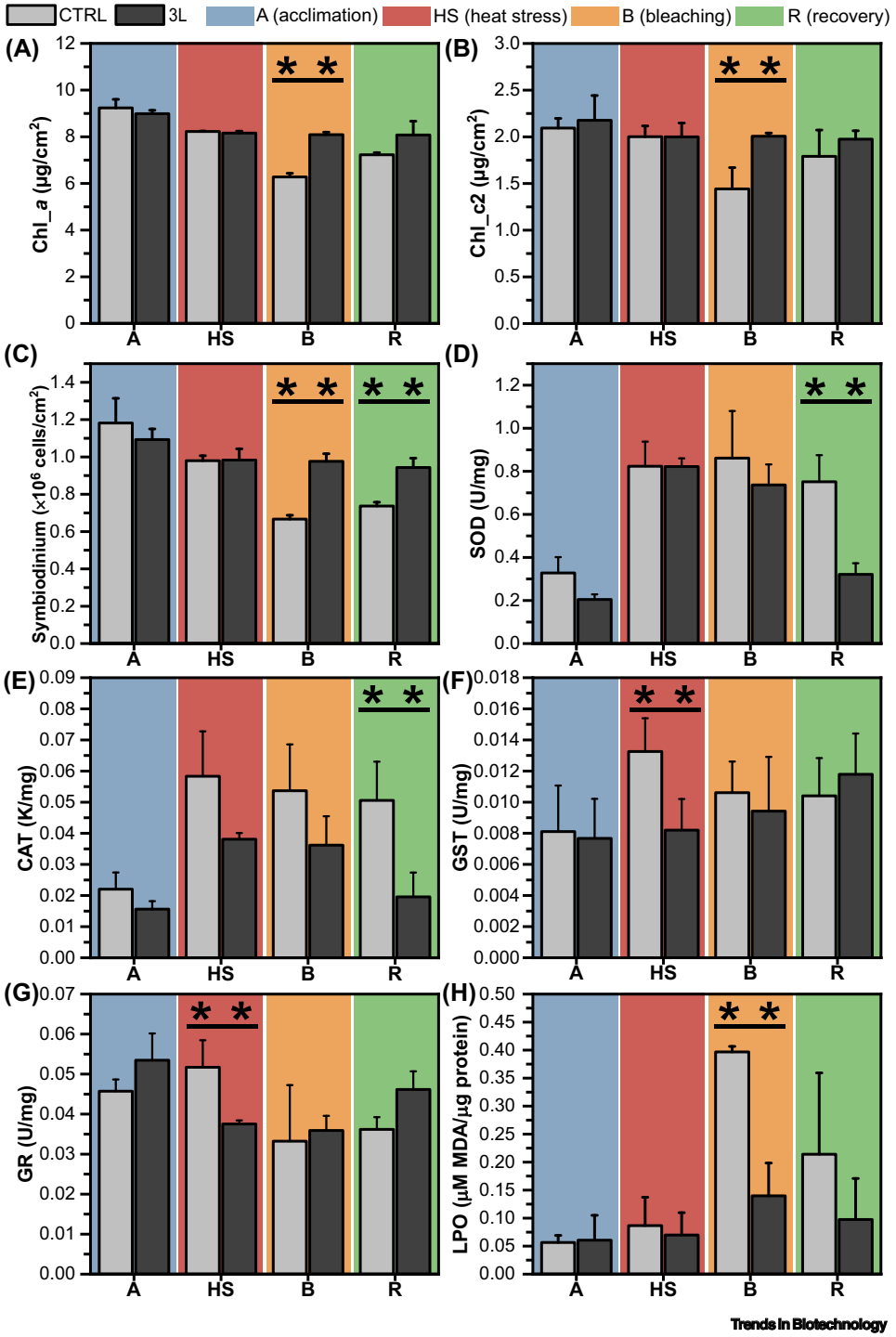


Figure 5. Results from molecular analysis of the induced thermal stress experimental setup: (A) chlorophyll *a* [*$P < 0.05$ CTRL vs. 3L; bleaching phase $P = 0.000077$, effect size (η^2) = 0.977], (B) chlorophyll c_2 [*$P < 0.05$ CTRL vs. 3L; bleaching phase $P = 0.013$, effect size (η^2) = 0.834], (C) Symbiodiniaceae cell density [*$P < 0.05$ CTRL vs. 3L; bleaching phase $P = 0.00029$, effect size (η^2) = 0.912; recovery phase P =

(Figure legend continued at the bottom of the next page.)

and 0.051 K/mg, respectively. By contrast, the CAT values for the treated corals in the heat stress, bleaching, and recovery phases were 0.038 K/mg, 0.036 K/mg, and 0.020 K/mg, respectively, resulting in a statistically significant difference in the recovery phase (*P = 0.022, η^2 = 0.757). GST showed a peak in expression during the HS phase in the untreated samples (≈0.013 U/mg), and then stabilized in the B and R phases at ≈0.010 U/mg. The treatment conferred statistically significant protection in the HS phase, with GST levels of ≈0.008 U/mg (*P = 0.048, η^2 = 0.541), and then slightly increased in the other two phases (B ≈ 0.009 U/mg; R ≈ 0.010 U/mg), reaching comparable values to the untreated corals. Finally, GR levels increased in the HS phase for the untreated samples (≈0.051 U/mg) and were statistically different from the treated corals (≈0.036 U/mg) (*P = 0.024, η^2 = 0.744). In the B and R phases, no significant differences or trends were observed for this enzyme.

Oxidative stress generates an overproduction of ROS, which can damage cellular components such as DNA, proteins, and lipids. Interaction of ROS with lipids leads to LPO and, for this reason, LPO is considered a clear and ubiquitous sign of ROS-induced cellular damage [56,57].

As a final biomarker of coral health status and thermally induced damage, LPO levels were evaluated in all phases and experimental groups, and the results are reported in Figure 5H. In the A and HS phases, LPO levels did not show significant variations (A ≈ 0.06 μM MDA/μg protein and HS ≈ 0.07 μM MDA/μg protein for both treated and untreated corals in the two phases), probably due to the time required for ROS to induce damage. During the B phase, it became evident that heat stress produced large amounts of ROS, and consequently, the untreated corals presented LPO values of ≈0.40 μM MDA/μg protein, while the samples treated with the Cur-β-CD nanocomplex had LPO levels of ≈0.14 μM MDA/μg protein (*P = 0.008, η^2 = 0.588). Finally, in the R phase, the untreated corals still showed more severe damage, with LPO values of ≈0.22 μM MDA/μg protein, compared with ≈0.10 μM MDA/μg protein in the treated corals.

The overproduction of enzymes, together with the decreased levels of chlorophylls and Symbiodiniaceae cells, and increased LPO, which are considered inter- and intramolecular signals of ROS damage and stress, confirmed the suitability of this induced thermal-stress model [58–60]. An overall positive effect of the three-layered material used for the administration of the cur-β-CD nanocomplex may be observed across all biomarkers considered. These observed differences in antioxidant enzyme activities, particularly during heat stress and recovery phases, could suggest that treated corals require lower enzyme activity than controls due to the ROS-scavenging effect of the β-CD–curcumin-complexed nanocarrier. However, this is only one possible explanation, and other scenarios, such as suppression of the stress response, cannot be excluded. Further experiments, including direct measurement of ROS levels or additional functional assessments, would be needed to confirm this hypothesis. All the significant differences, relative P-values, and η^2 are reported in Table S2 in the Supplemental information online. Finally, a schematic representation of heat effects and three-layered film applications is reported in Figure 6.

0.0028, effect size (η^2) = 0.890], (D) SOD [*P < 0.05 CTRL vs. 3L; recovery phase P = 0.0051, effect size (η^2) = 0.931], (E) CAT [*P < 0.05 CTRL vs. 3L; recovery phase P = 0.022, effect size (η^2) = 0.757], (F) GST [*P < 0.05 CTRL vs. 3L; heat stress phase P = 0.048, effect size (η^2) = 0.541], (G) GR [*P < 0.05 CTRL vs. 3L; heat stress phase P = 0.024, effect size (η^2) = 0.744], and (H) LPO [*P < 0.05 CTRL vs. 3L; bleaching phase P = 0.008, effect size (η^2) = 0.588] for both control corals and three-layered film system-treated corals in each phase of the coral bleaching experiment. Total number of corals analyzed: n = 24. Total number of corals analyzed after each phase: n = 3. CAT: catalase; CTRL: control; GR: glutathione reductase; GST: glutathione S-transferase; LPO: lipid peroxidation; MDA: malondialdehyde; SOD: superoxide dismutase.

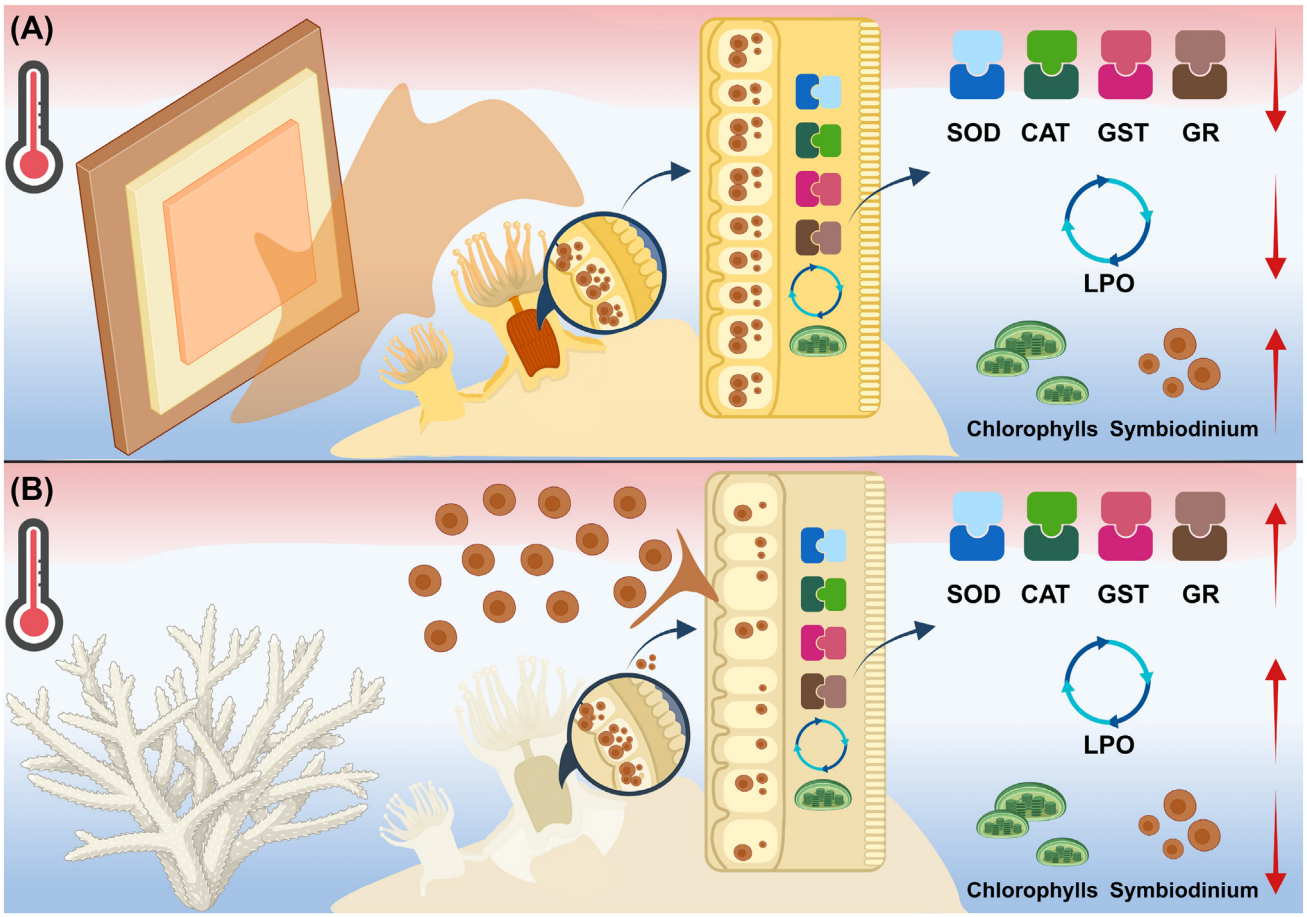


Figure 6. Schematic representation and summary of the effects of the heat stress model on biomarkers. These include chlorophylls, Symbiodiniaceae, antioxidant enzymes (SOD, CAT, GST, and GR), and lipid peroxidation (LPO). (A) *In vivo* application of the antioxidant three-layered underwater film system. From left to right, the absorption of cur-β-CD within coral cells is shown. A hypothetical schematic cross-section of coral tissue includes a magnified view of the gastrodermis and symbiosomes, illustrating the potential intracellular effects of curcumin on the selected biomarkers. (B) A schematic representation of the condition without application of the drug delivery system, showing the hypothetical intracellular effects of heat stress on the same biomarkers. CAT: catalase; cur-β-CD: curcumin–β-cyclodextrin; GR: glutathione reductase; GST: glutathione S-transferase; SOD: superoxide dismutase.

Replication and statistical considerations

Each coral fragment represents an independent biological replicate (n = 12 per experimental group, derived from six parent colonies). Molecular analyses were performed in technical triplicate per fragment. Statistical analyses are presented for indicative purposes, as the use of a single tank per treatment prevents full separation of tank-level effects (as indicated in 'Discussion' section). *P*-values indicate trends rather than definitive proof. However, η^2 were also calculated to assess whether the three-layered film system treatment had effects that were not only statistically significant—corroborating the significant *P*-values obtained—but also biologically meaningful. Indeed, effect size estimates (η^2) indicated that treatment strongly influenced most biomarkers. Very large effect sizes were observed for SOD (η^2 = 0.931), Chl_*a* (η^2 = 0.977), Symbiodiniaceae density (η^2 = 0.912), and Chl_c_2 (η^2 = 0.834), indicating that treatment explained a substantial proportion of the observed variability. CAT (η^2 = 0.757), GR (η^2 = 0.744), GST (η^2 = 0.541), and LPO (η^2 = 0.588) also showed large effect sizes, supporting a strong physiological response to treatment.

Discussion

The global decline of coral reefs is driven by natural and human factors, notably climate-induced heat stress, which causes bleaching and disease [61]. Emerging technologies based on materials science, including passive structures [25,62,63], eco-friendly materials [20,22,24], underwater drug delivery systems [23,64], materials for coral larvae settlement and algal antifouling [65–67], and microbiome manipulation [68,69] are enhancing coral protection and restoration efforts. Among these, natural antioxidants show promise in mitigating oxidative stress linked to bleaching [26,27]. However, this approach remains less explored compared with genetic or other material-based strategies, mainly due to challenges in efficient drug delivery.

To enhance the targeted administration of bioactive compounds in underwater environments, we propose an eco-friendly, three-layered film system as a versatile delivery platform. In this study, the system was loaded with curcumin, which was selected as a model antioxidant agent to mitigate oxidative stress in corals. The low solubility of curcumin in water was overcome by complexation with β-cyclodextrin, a crucial step to improve its solubility in the diffusion medium, potentially enhancing absorption and bioavailability and ultimately increasing therapeutic efficacy. In its dried state, the three-layered film system possessed a solid yet flexible consistency and exhibited hydrogel-like behavior when immersed in seawater. Because the material contains natural polysaccharides, contact with saltwater ions promotes either spontaneous crosslinking or a pH-induced decrease in solubility, both of which prolong its underwater stability. Each layer was engineered to degrade at distinct rates, thereby enabling a continuous and gradual release of curcumin, which was incorporated into the first two layers of the film. As demonstrated, the hydrophobic, zein-based third layer provided structural stability, ductility, and flexibility to the system, as well as directional diffusion of most of the drug, facilitating the targeted delivery of the antioxidant toward the coral target. This property potentially maximizes therapeutic efficacy while minimizing dispersion into the surrounding environment.

To further support safe future deployment in real open-field conditions, the system's complete biodegradability was investigated. Environmental biodegradation was confirmed through biochemical oxygen demand tests, demonstrating that microorganisms can digest all components of the system. This ensures that, whether in aquaria or natural reef settings, the material does not persist as a pollutant, in contrast to plastic-based objects commonly used in coral restoration, enabling a one-shot, eco-friendly application without the need for retrieval.

Outcomes from *in vivo* experiments on corals suggest that the three-layered film system may contribute to mitigating oxidative stress in *S. pistillata* fragments, as evidenced by the high chlorophyll content and Symbiodiniaceae density, together with the modulation of key oxidative stress markers. These effects are likely associated with the ROS-scavenging activity of curcumin—a key feature of this molecule, as confirmed by ABTS assay results—which may also modulate the coral antioxidant enzymatic responses, as noted in analyses of bleaching biomarkers. Importantly, the use of a single tank per experimental condition did not allow separation of tank-level effects; therefore, statistical analyses should be interpreted as indicative trends rather than definitive evidence. Nevertheless, the present findings are consistent with previous observations reported by Contardi and coworkers [27], in which curcumin-based treatments also demonstrated antioxidant effects in thermally stressed *S. pistillata* fragments under different experimental conditions. In both studies, a single application of curcumin-loaded film systems was sufficient to induce measurable antioxidant responses, without visible macroscopic side effects such as mucus overproduction or tissue necrosis. However, in our first prototype, 50 mg of curcumin were loaded into a single-layer film that exhibited isotropic drug release and was directly wrapped around the coral fragments. In that study, we demonstrated that modulation of the ratio between a

hydrophilic (PVP) and a hydrophobic (zein) polymer enabled control over curcumin release for up to 24 h. Instead, in the present work, we developed a three-layered film system with anisotropic drug release, increasing the curcumin loading to 350 mg. This design was intended both to evaluate the effects of a higher antioxidant load and to achieve a more sustained release profile over time through drug encapsulation within a multilayer system.

Future studies will further investigate the curcumin dose–effect response, the release under different flow regimes, the interaction with coral-associated microbiomes, and potential cumulative effects in scenarios involving multiple film deployments. Collectively, these findings support the potential for controlled underwater drug-delivery approaches as emerging tools for further investigation in field applications, including coral nurseries and other underwater environments.

Regarding the transition of this technology from laboratory scale to a commercial safety product, we want to highlight some important features of the designed material. All components used in the three-layer film system are low-cost, widely available, and already in common use in the food, cosmetic, and pharmaceutical sectors. In addition, the selected compounds are biodegradable under marine conditions and do not currently carry environmental hazard classifications in their safety data sheets. Curcumin, a food additive (E100) approved by the European Food Safety Authority, was selected not only for its availability, low toxicity, and established industrial use but also for its well-known radical-scavenging antioxidant activity attributed to its unique chemical structure.

Although the present study focused on the small-scale production of the system due to its final application in controlled aquaria environments, the industrially relevant fabrication techniques adopted, such as solvent casting, rod coating, and spray coating—commonly employed in pharmaceutical and food-packaging technology—suggest a quick transition to more scalable manufacturing conditions. Considering the overall prototype fabrication, characterization, and validation at the laboratory scale and in an initial relevant environment (*in vivo* experimentation on corals), the technology can currently be positioned within TRLs 4 and 5.

The absence of evidence of environmental toxicity in the selected materials, together with preliminary studies investigating the effects of curcumin on other marine organisms, including the amphibious freshwater fish *Anabas testudineus* and adult zebrafish [70–72], supports further validation under relevant environmental conditions, including low- and high-energy reef ecosystems. In this regard, ongoing studies by our group in the Maldives are evaluating the system under natural reef conditions. A preliminary photograph showing the application of the three-layered film system on *Acropora* and *Porites* corals in the Maldives is provided in Figure S11 in the Supplemental information online, suggesting that the material maintained its structural integrity after 1 week underwater. However, these observations were not obtained under a controlled experimental design and should, therefore, be considered preliminary indications that support future field validation rather than validated experimental results.

Owing to its adaptable composition and fabrication process, the material can be produced and adapted in different sizes and shapes according to specific operational requirements. Moreover, for large-scale applications, the material is intended to be applied primarily in human-made structures, ranging from aquaria to underwater structures used for coral restoration.

Therefore, as a prospective application in the coral restoration field, the three-layered system could potentially be applied by a diver operator across all structures currently present at most coral restoration sites, such as nurseries, spiders, and underwater aquaria for micro-

fragmentation [19,73], as schematically shown in Figure 7. Such material could be used in the case of heat waves for the prevention of bleaching, as a first-aid tool, or as a repeated or seasonal deployment during chronic heat-stress events. Next steps should focus on field-scale validation and long-term monitoring to optimize system performance under different environmental conditions (TRLs 6–7). In coral nurseries, for example, water flow dynamics and the distance between the delivery platform and coral colonies will likely represent critical parameters influencing therapeutic efficacy and release efficiency.

Beyond reef restoration applications, the system may also be useful in indoor aquarium environments, where local bleaching frequently occurs because of excessive light exposure [74–76]. The three-layered material can be easily and effectively applied in the closed environment of tanks to restore normal homeostasis in colonies under stress or experiencing local bleaching.

Finally, the platform could be adapted for the delivery of additional antioxidants, potentially extending its application to other marine organisms affected by oxidative stress or requiring localized administration of therapeutic agents. This technology may represent a versatile underwater

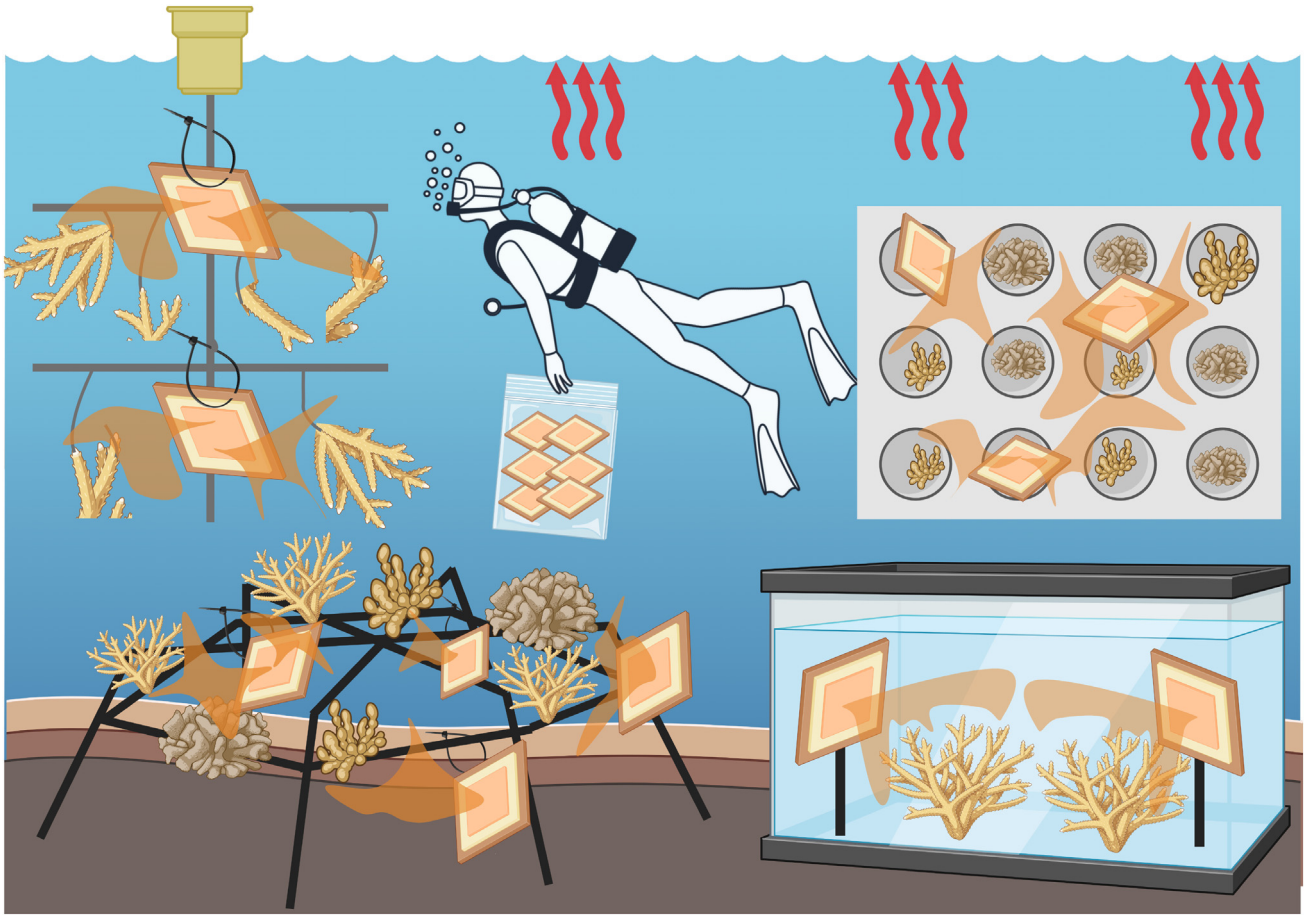


Figure 7. Schematic representation of the possible uses of the three-layer underwater film system: outdoor coral restoration (nurseries, top left; spiders/reef stars, bottom left), microfragmentation (top right), and aquaria (bottom right).

platform for the controlled delivery of 'active compounds' in marine biotechnology, conservation strategies, and underwater therapeutic applications.

In summary, the functionalized three-layered film system (i) provides a tunable, continuous, and directional release of the curcumin–β-cyclodextrin-complexed nanocarrier; (ii) mitigates oxidative stress responses associated with thermal stress under controlled conditions without requiring direct contact with the coral skeleton; and (iii) exhibits promising mechanical properties and potential for adaptation across different coral morphologies in aquarium-based settings, warranting further investigation in real field environments.

Concluding remarks

In conclusion, we demonstrated that the present three-layered film system can ensure tunable and directional underwater release of curcumin, enhancing coral's capacity to withstand thermal stress and suggests its application in aquaria, open-field environments, and existing artificial reef structures (Figure 7) to mitigate coral bleaching. This technology has progressed from a low TRL (conceptual stage) to a medium TRL through experimental validation, and future development should focus on two key aspects: in-field application and fabrication scale-up (see Outstanding questions). Specifically, further studies should assess the long-term performance and repeated application of the material in natural environments, including its positioning and anchoring, and determine the number of units required for effective application during large-scale coral bleaching events, potentially supported by trained robotic systems. A second bottleneck is the scale-up of the fabrication process. The three fabrication methodologies—solvent casting, rod coating, and spray drying—have thus far been validated only at the laboratory scale. Scaling up will require optimization of the formulation and process parameters for each layer to facilitate film pulling, solvent evaporation, and appropriate solution expulsion through the nozzle, enabling continuous production of larger and more uniform film areas while reducing batch-to-batch variability. This transition would increase manufacturing throughput and provide the material quantities required for future large-scale field deployment and coral restoration applications.

In alignment with the 2030 Agenda for Sustainable Development, this approach contributes to climate resilience and marine conservation, addressing key targets of the Sustainable Development Goals (SDGs) 12 (Responsible Consumption and Production), 13 (Climate Action), and 14 (Life Below Water).

STAR★METHODS

Detailed methods are provided in the online version of this paper and include the following:

- KEY RESOURCES TABLE
- EXPERIMENTAL MODEL AND STUDY PARTICIPANT DETAILS
  - Film application on corals
- METHOD DETAILS
  - Materials
  - Preparation of films
  - Scanning electron microscopy and energy-dispersive X-ray spectroscopy
  - Curcumin–(2-hydroxypropyl)-β-cyclodextrin complexation
  - Attenuated total reflection-Fourier transform infrared (ATR-FTIR) spectroscopy
  - Mechanical properties
  - Rheological tests
  - Swelling properties
  - Gel fraction properties
  - Drug release studies

Outstanding questions

How can the biopolymer-based multilayer film system be further optimized to enhance drug loading, release kinetics, and stability for long-term deployment in dynamic reef environments?

What are the long-term ecological impacts, degradation pathways, and scalability considerations for deploying such biomaterials directly in natural reef ecosystems?

How can this technology be integrated with emerging reef restoration tools (e.g., assisted evolution, microbiome engineering, and thermal-resistant symbiont inoculation) to create synergistic and more resilient conservation strategies?

What are the technical, regulatory, and socioeconomic barriers to scaling this intervention from aquaria trials to field deployment, and how can alignment with SDG targets be used to guide responsible translation?

- Unidirectionality drug release studies
- ABTS free radical cation scavenging assay
- Biochemical oxygen demand

- QUANTIFICATION AND STATISTICAL ANALYSIS
  - Molecular analysis
    - Quantification of chlorophyll *a* and c_2
    - Symbiodiniaceae density
  - Oxidative stress analysis
    - Protein extraction
    - Superoxide dismutase activity assay
    - Catalase activity assay
    - Glutathione S-transferase activity assay
    - Glutathione reductase activity assay
    - Lipid peroxidation
- Statistical analysis

RESOURCE AVAILABILITY

Lead contact

Requests for further information and resources should be directed to and will be fulfilled by the lead contact, Camilla Rinaldi (camilla.rinaldi@iit.it).

Materials availability

This study did not generate new unique reagents.

Data and code availability

Data have been deposited in Zenodo and are publicly available at https://doi.org/10.5281/zenodo.22313775. This paper does not report any original code. Any additional information required to reanalyze the data reported in this paper is available from the lead contact upon request.

Author contributions

C.R.: conceptualization, data curation, formal analysis, investigation, visualization, writing – original draft, and writing – review & editing. M.C.: conceptualization, data curation, formal analysis, investigation, visualization, supervision, writing – original draft, and writing – review & editing. V.I.: formal analysis, investigation, and writing – original draft. G.C., L.R., V.S., M.F., E.B., E.M., and D.S. formal analysis and investigation. S.L.: investigation and resources. P.G.: resources and writing – review & editing. S.M.: conceptualization, resources, supervision, writing – original draft, and writing – review & editing. A.A.: conceptualization, resources, supervision, funding acquisition, and writing – review & editing.

Acknowledgments

The authors would like to declare that part of this research was funded under the National Recovery and Resilience Plan, Mission 4, Component 2, Investment 1.4—call for tender no. 3138 of 16 December 2021, rectified by Decree no. 3175 of 18 December 2021 of the Italian Ministry of University and Research, and funded by the European Union – NextGenerationEU. Project code: CN_00000033; Concession Decree no. 1034 of 17 June 2022, adopted by the Italian Ministry of University and Research; CUP: J33C22001200001; project title 'National Biodiversity Future Center (NBFC)'. This work is part of the 'Technologies for Sustainability' flagship program of the Italian Institute of Technology.

We would also like to acknowledge BioRender (http://biorender.com/), which has been used to produce the Graphical Abstract, as well as Figures 6 and 7 of the main manuscript.

Declaration of interests

The authors declare no competing interests.

Supplemental information

Supplementary information associated with this article can be found online at https://doi.org/10.1016/j.tibtech.2026.09.012.

References

1. Eddy, T.D. *et al.* (2021) Global decline in capacity of coral reefs to provide ecosystem services. *One Earth* 4, 1278–1285
2. Hughes, D.J. *et al.* (2020) Coral reef survival under accelerating ocean deoxygenation. *Nat. Clim. Chang.* 10, 296–307
3. Costanza, R. *et al.* (2014) Changes in the global value of ecosystem services. *Glob. Environ. Chang.* 26, 152–158
4. Pandolfi, J.M. *et al.* (2003) Global trajectories of the long-term decline of coral reef ecosystems. *Science* 301, 955–958
5. Baker, A.C. *et al.* (2008) Climate change and coral reef bleaching: an ecological assessment of long-term impacts, recovery trends and future outlook. *Estuar. Coast. Shelf Sci.* 80, 435–471
6. LaJeunesse, T.C. *et al.* (2018) Systematic revision of Symbiodiniaceae highlights the antiquity and diversity of coral endosymbionts. *Curr. Biol.* 28, 2570–2580.e6
7. Gray, V. (2007) Climate change 2007: the physical science basis summary for policymakers. *Energy Environ.* 18, 433–440
8. Phinney, J.T. (2006) *Coral Reefs and Climate Change: Science and Management*, 61. American Geophysical Union
9. Eddy, T.D. *et al.* (2018) Historical baselines of coral cover on tropical reefs as estimated by expert opinion. *PeerJ* 6, e4308
10. Hughes, T.P. *et al.* (2017) Coral reefs in the Anthropocene. *Nature* 546, 82–90
11. Sun, H. *et al.* (2023) New insights into microbial and metabolite signatures of coral bleaching. *Sci. Total Environ.* 892, 164258
12. Weis, V.M. (2008) Cellular mechanisms of cnidarian bleaching: stress causes the collapse of symbiosis. *J. Exp. Biol.* 211, 3059–3066
13. Davy, S.K. *et al.* (2012) Cell biology of cnidarian-dinoflagellate symbiosis. *Microbiol. Mol. Biol. Rev.* 76, 229–261
14. Helgoe, J. *et al.* (2024) Triggers, cascades, and endpoints: connecting the dots of coral bleaching mechanisms. *Biol. Rev.* 99, 715–752
15. Downs, C.A. *et al.* (2002) Oxidative stress and seasonal coral bleaching. *Free Radic. Biol. Med.* 33, 533–543
16. Lesser, M.P. (2011) Coral bleaching: causes and mechanisms. In *Coral Reefs: An Ecosystem in Transition* (Dubinsky, Z. and Stambler, N., eds), pp. 405–421, Springer
17. Peixoto, R.S. *et al.* (2024) The critical role of coral reef restoration in a changing world. *Nat. Clim. Chang.* 14, 1219–1222
18. Bayraktarov, E. *et al.* (2019) Motivations, success, and cost of coral reef restoration. *Restor. Ecol.* 27, 981–991
19. Boström-Einarsson, L. *et al.* (2020) Coral restoration – a systematic review of current methods, successes, failures and future directions. *PLoS One* 15, e0226631
20. Wangpraseurt, D. *et al.* (2022) Bioprinted living coral microenvironments mimicking coral-algal symbiosis. *Adv. Funct. Mater.* 32, 2202273
21. Allahgholi, A. (2014) Coral reef restoration – a guide to effective rehabilitation techniques. *Ecol. Restor.* 56
22. Zych, A. *et al.* (2024) Underwater quick-hardening vegetable oil-based biodegradable putty for sustainable coral reef restoration and rehabilitation. *Adv. Sustainable Syst.* 8, 2400110
23. Scribano, V. *et al.* (2025) Eco-friendly active film and sealant for underwater drug delivery to diseased corals. *One Earth* 8, 101356
24. Corigliano, G. *et al.* (2025) Active biopaste for coral reef restoration. *Adv. Mater.* 37, 2502078
25. Santoro, E.P. *et al.* (2021) Coral microbiome manipulation elicits metabolic and genetic restructuring to mitigate heat stress and evade mortality. *Sci. Adv.* 7, eabg3088
26. Roger, L.M. *et al.* (2022) Engineered nanoceria alleviates thermally induced oxidative stress in free-living *Breviolum minutum* (Symbiodiniaceae, formerly clade B). *Front. Mar. Sci.* 9, 960173
27. Contardi, M. *et al.* (2023) Biodegradable zein-based biocomposite films for underwater delivery of curcumin reduce thermal stress effects in corals. *ACS Appl. Mater. Interfaces* 15, 33916–33931
28. Li, L. *et al.* (2014) Carrageenan and its applications in drug delivery. *Carbohydr. Polym.* 103, 1–11
29. Ngouémazong, E.D. *et al.* (2015) The emulsifying and emulsion-stabilizing properties of pectin: a review. *Compr. Rev. Food Sci. Food Saf.* 14, 705–718
30. Muxika, A. *et al.* (2017) Chitosan as a bioactive polymer: processing, properties and applications. *Int. J. Biol. Macromol.* 105, 1358–1368
31. Tortorella, S. *et al.* (2021) Zein as a versatile biopolymer: different shapes for different biomedical applications. *RSC Adv.* 11, 39004–39026
32. Jahed, V. *et al.* (2014) NMR (^{1}H, ROESY) spectroscopic and molecular modelling investigations of supramolecular complex of β-cyclodextrin and curcumin. *Food Chem.* 165, 241–246
33. Jiang, L. *et al.* (2022) Preparation and characterization of curcumin/β-cyclodextrin nanoparticles by nanoprecipitation to improve the stability and bioavailability of curcumin. *Lwt* 171, 114149
34. Singh, R. *et al.* (2010) Studies of curcumin and curcuminoids. XXXVI. The stoichiometry and complexation constants of cyclodextrin complexes as determined by the phase-solubility method and UV–Vis titration. *J. Incl. Phenom. Macrocycl. Chem.* 66, 335–348
35. Martínez-Guerra, J. *et al.* (2022) On the curcumin and β-cyclodextrin interaction in aqueous media. Spectrophotometric and electrochemical study. *ChemElectroChem* 9, e202101534
36. Prado-Fernández, J. *et al.* (2003) Quantitation of κ-, ι- and λ-carrageenans by mid-infrared spectroscopy and PLS regression. *Anal. Chim. Acta* 480, 23–37
37. Güzel, M. and Akpınar, Ö. (2019) Valorisation of fruit by-products: production characterization of pectins from fruit peels. *Food Bioprod. Process.* 115, 126–133
38. Mireles, L.K. *et al.* (2020) Physicochemical characterization of polyvinyl pyrrolidone: a tale of two polyvinyl pyrrolidones. *ACS Omega* 5, 30461–30467
39. Kolev, T.M. *et al.* (2005) DFT and experimental studies of the structure and vibrational spectra of curcumin. *Int. J. Quantum Chem.* 102, 1069–1079
40. Nikolić, V.D. *et al.* (2014) Photostability of piroxicam in the inclusion complex with 2-hydroxypropyl-β-cyclodextrin. *Hem. Ind.* 68, 107–116
41. Bölgen, N. *et al.* (2016) Extraction and characterization of chitin and chitosan from blue crab and synthesis of chitosan cryogel scaffolds. *J. Turk. Chem. Soc. A: Chem.* 3, 131–144
42. Corradini, E. *et al.* (2014) Recent advances in food-packing, pharmaceutical and biomedical applications of zein and zein-based materials. *Int. J. Mol. Sci.* 15, 22438–22470
43. Byler, D.M. and Susi, H. (1986) Examination of the secondary structure of proteins by deconvolved FTIR spectra. *Biopolymers* 25, 469–487
44. Navarra, G. *et al.* (2016) Heat- and pH-induced BSA conformational changes, hydrogel formation and application as 3D cell scaffold. *Arch. Biochem. Biophys.* 606, 134–142
45. Erickson, D.P. *et al.* (2020) Corn zein undergoes conformational changes to higher β-sheet content during its self-assembly in an increasingly hydrophilic solvent. *Int. J. Biol. Macromol.* 157, 232–239
46. Xie, F. (2023) Biopolymer-based multilayer films and coatings for food preservation: an update of the recent development. *Curr. Food. Sci. Technol. Rep.* 1, 1–12
47. Li, D. *et al.* (2017) Pectin gels cross-linked by Ca^{2+}: an efficient material for methylene blue removal. *J. Mol. Liq.* 238, 36–42
48. Wurm, F. *et al.* (2020) Multivalent ions as reactive crosslinkers for biopolymers—a review. *Molecules* 25, 1840
49. Chaichi, M. *et al.* (2019) Water resistance and mechanical properties of low methoxy-pectin nanocomposite film responses to interactions of Ca^{2+} ions and glycerol concentrations as crosslinking agents. *Food Chem.* 293, 429–437
50. Keppeler, S. *et al.* (2009) Cross-linked carrageenan beads for controlled release delivery systems. *Carbohydr. Polym.* 78, 973–977
51. Li, L. *et al.* (2019) Ionically cross-linked sodium alginate/ -carrageenan double-network gel beads with low-swelling, enhanced mechanical properties, and excellent adsorption performance. *Chem. Eng. J.* 372, 1091–1103
52. Mohamadnia, Z. *et al.* (2008) Ionically cross-linked carrageenan-alginate hydrogel beads. *J. Biomater. Sci. Polym. Ed.* 19, 47–59
53. Cataldo, S. *et al.* (2009) Solubility and acid-base properties and activity coefficients of chitosan in different ionic media and at different ionic strengths, at T = 25°C. *J. Mol. Liq.* 148, 120–126

54. Miyaji, K. *et al.* (2023) Biodegradation of various forms of cellulose and chitin in natural waters with different salinity. *Polym. Degrad. Stab.* 215, 110423
55. Tsuji, H. and Suzuyoshi, K. (2002) Environmental degradation of biodegradable polyesters 2. Poly (ε-caprolactone), poly [(R)-3-hydroxybutyrate], and poly (L-lactide) films in natural dynamic seawater. *Polym. Degrad. Stab.* 75, 357–365
56. Nielsen, D.A. and Petrou, K. (2023) Lipid stores reveal the state of the coral-algae symbiosis at the single-cell level. *ISME Commun.* 3, 29
57. Lesser, M.P. (2006) Oxidative stress in marine environments: biochemistry and physiological ecology. *Annu. Rev. Physiol.* 68, 253–278
58. Downs, C.A. *et al.* (2000) A molecular biomarker system for assessing the health of coral (*Montastraea faveolata*) during heat stress. *Mar. Biotechnol.* 2, 533–544
59. Montalbetti, E. *et al.* (2023) Mucilage-induced necrosis reveals cellular oxidative stress in the Mediterranean gorgonian *Paramuricea clavata*. *J. Exp. Mar. Biol. Ecol.* 559, 151839
60. Seveso, D. *et al.* (2024) *The Cellular Stress Response and Physiological Adaptations of Corals Subjected to Environmental Stressors and Pollutants, Volume II*, Vol. 15. Frontiers Media SA
61. Côté, I.M. *et al.* (2005) Measuring coral reef decline through meta-analyses. *Phil. Trans. R. Soc. B: Biol. Sci.* 360, 385–395
62. Albalawi, H.I. *et al.* (2021) Sustainable and eco-friendly coral restoration through 3D printing and fabrication. *ACS Sustain. Chem. Eng.* 9, 12634–12645
63. Levy, N. *et al.* (2022) Emerging 3D technologies for future reformation of coral reefs: enhancing biodiversity using biomimetic structures based on designs by nature. *Sci. Total Environ.* 830, 154749
64. Contardi, M. *et al.* (2020) Treatment of coral wounds by combining an antiseptic bilayer film and an injectable antioxidant biopolymer. *Sci. Rep.* 10, 988
65. Contardi, M. *et al.* (2021) Marine fouling characteristics of biocomposites in a coral reef ecosystem. *Adv. Sustainable Syst.* 5, 2100089
66. Levy, N. *et al.* (2025) Microbial living materials promote coral larval settlement. *PNAS Nexus* 4, pgaf268
67. Karimi, Z. *et al.* (2025) Mitigating algal competition with fouling-prevention coatings for coral restoration and reef engineering. *ACS Sustain. Chem. Eng.* 13, 5808–5817
68. Rosado, P.M. *et al.* (2019) Marine probiotics: increasing coral resistance to bleaching through microbiome manipulation. *ISME J.* 13, 921–936
69. Thatje, S. (2024) Preventing bleaching in tropical corals by using thermally resilient symbiont zooxanthellae: all hands-on deck! *Mar. Ecol.* 45, e12843
70. Manju, M. *et al.* (2009) Curcumin analogue inhibits lipid peroxidation in a freshwater teleost, *Anabas testudineus* (Bloch)—an in vitro and in vivo study. *Fish Physiol. Biochem.* 35, 413–420
71. Manju, M. *et al.* (2013) Protective effect of dietary curcumin in *Anabas testudineus* (Bloch) with a special note on DNA fragmentation assay on hepatocytes and micronucleus assay on erythrocytes in vivo. *Fish Physiol. Biochem.* 39, 1323–1330
72. Coradini, K. *et al.* (2021) Free and nanoencapsulated curcumin prevents scopolamine-induced cognitive impairment in adult zebrafish. *J. Drug Delivery Sci. Technol.* 66, 102781
73. Boström-Einarsson, L. *et al.* (2018) *Coral Restoration in a Changing World—A Global Synthesis of Methods and Techniques*, Reef and Rainforest Research Centre Ltd
74. Titlyanov, E.A. *et al.* (2001) Photo-acclimation dynamics of the coral *Stylophora pistillata* to low and extremely low light. *J. Exp. Mar. Biol. Ecol.* 263, 211–225
75. Bhagooli, R. and Hidaka, M. (2004) Photoinhibition, bleaching susceptibility and mortality in two scleractinian corals, *Platygyra ryukyuensis* and *Stylophora pistillata*, in response to thermal and light stresses. *Comp. Biochem. Physiol. A Mol. Integr. Physiol.* 137, 547–555
76. Levy, O. *et al.* (2016) Molecular assessment of the effect of light and heterotrophy in the scleractinian coral *Stylophora pistillata*. *Proc. Biol. Sci.* 283, 20153025
77. La Notte, L. *et al.* (2018) Fully-sprayed flexible polymer solar cells with a cellulose-graphene electrode. *Mater. Today Energy* 7, 105–112
78. La Notte, L. *et al.* (2018) Sprayed organic photovoltaic cells and mini-modules based on chemical vapor deposited graphene as transparent conductive electrode. *Carbon* 129, 878–883
79. Fadda, M. *et al.* (2022) Antioxidant coatings from elastomeric vinyl acetate-vinyl laurate copolymers with reduced bacterial adhesion. *Prog. Org. Coat.* 168, 106883
80. Voolstra, C.R. *et al.* (2020) Standardized short-term acute heat stress assays resolve historical differences in coral thermotolerance across microhabitat reef sites. *Glob. Chang. Biol.* 26, 4328–4343
81. Jeffrey, S.T. and Humphrey, G.F. (1975) New spectrophotometric equations for determining chlorophylls *a*, *b*, c_1 and c_2 in higher plants, algae and natural phytoplankton. *Biochem. Physiol. Pflanz.* 167, 191–194
82. Veal, C.J. *et al.* (2010) Increasing the accuracy of surface area estimation using single wax dipping of coral fragments. *Coral Reefs* 29, 893–897
83. Isa, V. *et al.* (2024) Physical and cellular impact of environmentally relevant microplastic exposure on thermally challenged *Pocillopora damicornis* (Cnidaria, Scleractinia). *Sci. Total Environ.* 918, 170651
84. Louis, Y.D. *et al.* (2016) *In hospite Symbiodinium* photophysiology and antioxidant responses in *Acropora muricata* on a coast-reef scale: implications for variable bleaching patterns. *Symbiosis* 68, 61–72
85. Vance, P.G. *et al.* (1972) Superoxide dismutase from *Streptococcus mutans*: isolation and characterization of two forms of the enzyme. *J. Biol. Chem.* 247, 4782–4786
86. Bergmeyer, H.U. (1974) *Methods of Enzymatic Analysis*, 3. Academic Press
87. Aebi, H. (1984) Catalase *in vitro*. *Methods Enzymol.* 105, 121–126
88. Hayes, J.D. and Strange, R.C. (2000) Glutathione S-transferase polymorphisms and their biological consequences. *Pharmacology* 61, 154–166
89. Wang, Y. *et al.* (2001) Antioxidant defense systems of two lipidopteran insect cell lines. *Free Radic. Biol. Med.* 30, 1254–1262
90. Gérard-Monnier, D. *et al.* (1998) Reactions of 1-methyl-2-phenylindole with malondialdehyde and 4-hydroxyalkenals. Analytical applications to a colorimetric assay of lipid peroxidation. *Chem. Res. Toxicol.* 11, 1176–1183

STAR★METHODS

KEY RESOURCES TABLE

Reagent or resource	Source	Identifier
Chemicals		
Pectin, from citrus peel	Sigma-Aldrich, Merck	Cat# P9135
Carrageenan	Sigma-Aldrich, Merck	Cat#C1013
Polyvinylpyrrolidone	Sigma-Aldrich, Merck	Cat#437190
Curcumin	Sigma-Aldrich, Merck	Cat#C1386
(2-Hydroxypropyl)-β-cyclodextrin	Sigma-Aldrich, Merck	Cat#H107
Chitosan	Sigma-Aldrich, Merck	Cat#C3646
Zein	Sigma-Aldrich, Merck	Cat#Z3625
Ethanol	Sigma-Aldrich, Merck	Cat#459844
Methanol	Sigma-Aldrich, Merck	Cat#34860
Acetic acid	Sigma-Aldrich, Merck	Cat#338826
Polyglycerine-6	SPIGA-NORD	https://www.spiganord.it/polyglycerols-pure-vegetable-polyglycerine-6_c2_p8/#1556026406822-69126593-c356
Software		
Origin Pro 2024	OriginLab, USA	https://www.originlab.com/demodownload.aspx
Biorender	Biorender	https://biorender.com/
ImageJ	Java	https://imagej.en.softonic.com/?ex=RAMP-3864.3&rex=true
Inkscape	GitHub	https://inkscape.org
Other		
Scanning Electron Microscope	JEOL, Tokyo, Japan	https://www.jeol.com/products/scientific/sem/
Fourier-transform infrared spectroscopy (FTIR)	Bruker	https://www.bruker.com/it/products-and-solutions/infrared-and-raman/ft-ir-research-spectrometers/vertex-research-ft-ir-spectrometer.html
Universal Testing System	Instron, USA	https://www.instron.com/en/products/testing-systems/universal-testing-systems/
Rheometer	Anton-Paar	https://www.anton-paar.com/it-it/prodotti/gruppo/reometro/
Uv-Visible Spectrophotometer	Walnut Creek, USA	https://www.agilent.com/en/product/molecular-spectroscopy/uv-vis-uv-vis-nir-spectroscopy/uv-vis-uv-vis-nir-systems/cary-60-uv-vis-spectrophotometer
Biochemical Oxygen Demand	FisherScientific	https://www.fishersci.it/shop/products/oxitop-i-respirometric-bod-measuring-system-8/16223561

EXPERIMENTAL MODEL AND STUDY PARTICIPANT DETAILS

Film application on corals

Following the experiment by Santoro and coworkers [25], a new coral bleaching setup was developed to evaluate the efficacy of the complete three-layered film system in mitigating heat stress in corals. The coral bleaching model was divided into four distinct phases: acclimation (A), heat stress (HS) (where the temperature was increased by 0.5°C daily), bleaching (B) (corals were maintained at 31°C for one week), and recovery (R) (temperature was gradually reduced by 1°C daily until reaching the original 25°C). Physicochemical parameters were continuously monitored and controlled. Water temperature was precisely adjusted using a 500W Aquamedic heater equipped with an external thermostat, maintaining a variation within ±0.1°C. A total of 24 coral fragments were cut from six visually distinct and spatially separated parent colonies of *Stylophora pistillata*, a model coral species. Representing independent biological units, these coral fragments were then acclimated and randomly distributed between two tanks (12 fragments per tank), corresponding to two experimental groups (untreated control group n = 12; film-treated group n = 12). The entire experiment was

conducted using a water bath setup, where twenty-liter coral tanks were placed inside a larger 500-liter tank under a 13-hour light and 11-hour dark cycle at 250 PAR. Each small tank was aerated individually using silicone tubing connected to the Genoa Aquarium air flow, and a 40% water change was performed three times per week.

In the treatment tank, coral fragments were surrounded by ~5 × 5 cm pieces of a three-layered substrate (Figure S10), while the control tank received no treatment. As mentioned above, each bilayer comprises 350 mg of curcumin distributed in 144 cm^2 of area. Assuming that the drug was homogeneously distributed within the system, each 5×5 cm cut piece with a total area of 25 cm^2 had a quantity of curcumin equal to ~70 mg. After the acclimation phase, during which corals were kept at 25°C, the temperature increased by 0.5°C per day until reaching a maximum of 31°C. The corals were then maintained at this temperature for a week before entering the recovery phase, where the temperature gradually decreased. To prevent excessive algal growth, water changes were performed every two days. Finally, at the end of each phase, three coral fragments, both from the treated and untreated groups, were collected for molecular analyses. The experiment was designed to induce thermal stress in corals strong enough to observe potential molecular differences between corals treated with the three-layered film system and untreated controls without causing mortality. To prevent complete bleaching, the temperature was reduced after seven days of exposure to 31°C (bleaching phase), initiating the recovery phase.

METHOD DETAILS

Materials

Pectin from citrus peel (galacturonic acid ≥ 74.0%) (dried basis), carrageenan, polyvinylpyrrolidone (PVP) (M_W = ~1,300,000 kDa), curcumin from *Curcuma longa* (turmeric) powder (Mw = 368,38 g/mol), (2-Hydroxypropyl)-β-cyclodextrin (Mw = ~1,460 Da), chitosan from crab shells (Mw = 600 kDa), Zein powder (average M_W = 20 kDa), ethanol, methanol, dimethyl sulfoxide (99,9%) and acetic acid (≥ 99.8%) were purchased from Sigma-Aldrich. Polyglycerine-6 was provided by SPIGA-NORD.

Preparation of films

To prepare layer 1, 288 mg of polyglycerine-6 (~10% w/w with respect to the total weight of pectin, carrageenan, and PVP) was dissolved in 56 mL of MilliQ water under stirring on a 60°C hot plate for 10 minutes. 140 mg of pectin powder was added to the glycerin solution and stirred for another 10 minutes at 60°C. Decreasing the temperature to 50°C, 2660 mg of carrageenan and 200 mg of PVP were added to the solution under stirring for no more than 2 hours.

Meanwhile, a 5 mL ethanol solution with a 1:2 w/w ratio of curcumin and (2-Hydroxypropyl)-β-cyclodextrin powders (175 mg of curcumin – 350 mg of βCD) was prepared and added to the original solution. After 2 hours, the solution was poured into square 12 × 12 cm Petri dishes and kept in the dark under an aspirated hood (20-23°C at 40-44% R.H.) overnight to eliminate solvents as schematically reported in Figure S1A.

For layer 2 preparation, 525 mg of chitosan and PVP were dissolved in 35 mL of an acidic aqueous solution (4% v/v acetic acid) and left under stirring at 70°C overnight (16 hours). Meanwhile, a 5 mL ethanol solution with a 1:2 w/w ratio of curcumin (2-Hydroxypropyl)-β-cyclodextrin powders (175 mg of curcumin – 350 mg of βCD) was prepared and added to the original solution. At least 35 mL of layer 2 solution was poured onto a well-dried layer 1 by using a Rod-coater system (model EZ coater EC-200; ChemInstruments) and left to dry overnight to eliminate solvents. Considering the total amount of solutions used to obtain the complete bilayer (56 mL from layer 1 and ~35 mL from layer 2), it can be assumed that each bilayer has a total amount of curcumin of ~ 350 mg. Preparation of the bilayer is schematically reported in Figure S1B.

Figure S1C shows the preparation of layer 3. 250 mg of Zein was dissolved first in 400 µL of DMSO, and then 2.3 mL of methanol and water were added to this solution and left under stirring for 1-2 hours. A 5% w/v zein solution was sprayed onto the bilayer system under a chemical hood using a dual-action commercial airbrush (Mecafer) supplied with compressed air at a pressure of 2 bar [77,78]. 10 mL of solution was deposited at a substrate-nozzle distance of 5 cm, flow rate of 1mL/min. For clarity, layer 1 is here called 'monolayer', layer 1 + layer 2 is referred to as 'bilayer system', and layer 1 + layer 2 + layer 3 as 'three-layered system'.

Scanning electron microscopy and energy-dispersive X-ray spectroscopy

The morphology of the obtained films was analyzed by Scanning Electron Microscopy (SEM), using a variable pressure JOEL JSM-649LA (JEOL, Tokyo, Japan) microscope equipped with a tungsten thermionic electron source and working in high vacuum mode,

with an acceleration voltage of 5 kV. The specimens were coated with a 10 nm thick film of gold utilizing a Cressington Sputter Coater – 208 HR (Cressington, Watford, UK).

Parallelly, to better highlight the differences between layer 1 and layer 2 in the bilayer, SEM-EDS (Scanning Electron Microscopy with Energy Dispersive X-ray Spectroscopy) analysis was performed. Measurements were conducted separately for layer 1 and layer 2, as well as for the bilayer. To maintain the integrity of the system and ensure a good quality of results, the ethanol-water dehydration treatment was followed before the fixation of the material.

Curcumin–(2-hydroxypropyl)-β-cyclodextrin complexation

To confirm the inclusion of curcumin within the 2-Hydroxypropyl-β-cyclodextrin hydrophobic cavity, solutions of ethanol with a 1:2 w/w ratio of curcumin and βCD and ethanol with just curcumin inside were left under stirring overnight. 1 mL of both solutions was added to an aqueous solution, and absorbance was measured with a Varian Cary 6000i Scan UV-visible spectrophotometer (Walnut Creek, California, USA).

Attenuated total reflection-Fourier transform infrared (ATR-FTIR) spectroscopy

Infrared spectra of the different layers of the system were acquired by using an ATR accessory (MIRacle ATR, PIKE Technologies) with a diamond crystal coupled to an FTIR spectrometer (Vertex 70v FTIR, Bruker). All spectra were recorded between 4000 and 600 cm^{-1}, with a resolution of 4 cm^{-1}, accumulating 64 scans. ATR-FTIR measurements were collected for monolayer, bilayer, and three-layered samples on both sides to better appreciate the successful overlap of each layer onto the other.

Mechanical properties

The mechanical properties of the different systems were determined by uniaxial tension tests on a dual-column universal testing machine Instron 3365 (Instron, Norwood, Massachusetts, USA). Films were cut into dog bone specimens (n = 10) with a width of 4 mm and an adequate length of 25 mm. Displacement was applied at a rate of 10 mm min^{-1}. Young's modulus, tensile stress at maximum load, and elongation at break were calculated from the stress-strain curves for the monolayer, bilayer, and three-layered film system. Before mechanical testing, dog-bone specimens were conditioned for 24 hours at 24 °C and 44% relative humidity (RH) in an Espec SH-262 environmental chamber.

Rheological tests

Rheological measurements were conducted using an Anton Paar Modular Compact Rheometer (MCR 302). Viscoelastic measurements were conducted on hydrated films using stress-controlled Rheometers equipped with a 40 mm PEEK plate, at a temperature of 28 ± 0.1 °C. Prior to analysis, a 5 mm diameter disk of monolayer, bilayer, and three-layered systems was immersed in seawater for 3 hours, then placed onto the rheometer plate. Tests were then repeated on samples immersed in seawater for 24 hours to evaluate the behavior of biofilms as hydrogels.

Amplitude sweep tests were conducted to determine the Linear Viscoelastic Region of each sample using a shear strain range from 10^{-4} to 1 at an angular frequency of 10 rad/s. Results are shown in Figure S6A,B. Subsequently, frequency sweep tests were performed on each sample within an angular frequency range of 0.1 to 1 rad/s, at a fixed shear strain of 10^{-3}.

Swelling properties

The films' aqueous liquid absorption and erosion behaviors were evaluated by placing 1 × 1 cm square of the samples (n = 5) in 12 mL of MilliQ water as well as seawater to mimic the underwater condition in terms of pH salts and composition. Samples were weighed at time zero and after 20 minutes, 40 minutes, 60 minutes, 2, 4, 6, and 24 hours, and the excess water was removed by placing the samples on filter paper. The swelling degree (SD, %) was calculated by using eq 1:

$$SD(\%) = \frac{W_t - W_i}{W_i} \times 100$$

where Wt corresponds to the weight of the swollen sample at the time t and Wi is the initial dry weight. Measurements were performed in triplicate.

Gel fraction properties

To evaluate the level of cross-linking, samples resulting from the swelling test (n = 5, 24 hours immersed in seawater) were dried under the hood overnight and weighed the day after. The percentage of gel fraction was calculated by using eq 2:

$$GF(\%) = \frac{Wi}{Wf} \times 100$$

Where Wi is the initial dry weight and Wf is the final one after being dried overnight. Measurements were performed in triplicate.

Drug release studies

The curcumin-βCD complexed nanocarrier release from each system was measured using a Varian Cary 6000i Scan UV–Visible spectrophotometer (Walnut Creek, California, USA). Curcumin in both MilliQ and seawater has a characteristic UV absorbance peak at 426 nm. A curcumin calibration curve was constructed using both MilliQ and seawater to extrapolate the molar extinction coefficient, leading to $\varepsilon = 1800\ cm^{-1}\ M^{-1}$. At time zero, t = 0 s, square samples of 1 × 1 cm were placed on the top part of a 6.5 mm Transwell with 8.0 µm pore polycarbonate membrane insert, TC-treated, w/lid, sterile, 48/cs immersed in 4 mL of seawater. Measurements were performed at specific time intervals. 2.5 mL of solution was taken out and replaced with the same amount of fresh medium at each time point (20 min, 40 min, 1h, 2h, 4h, 6h, 8h, 24h, 32h, 48h, 56h, 120h, 128h, 144h, 152h, 168h, 176h). All measurements were taken so that sinking conditions were maintained, and the validity of the Beer-Lambert law was reassured. The experiments were carried out in triplicate, and the data were expressed as a cumulative percentage. The entire Transwell Petri was sealed with Parafilm tape to avoid water evaporation.

Unidirectionality drug release studies

To verify the capacity of the complete three-layered film system to provide a good unidirectionality of cur-βCD toward the direction of the corals, a unidirectional drug release study was performed. Transwells were used to mimic the condition. The transwell structures were filled with 6.0 mm film disks, and 0.25 mL of seawater was then added. After this, the transwell was placed inside another well, firstly filled with 1.00 mL of seawater. The bottom part simulated the environment, while the top part simulated the coral's skeleton. The cur-βCD release from the system was measured using a Varian Cary 6000i Scan UV–Visible spectrophotometer (Walnut Creek, California, USA). Each volume from the two different compartments was collected at each time point (20 min, 40 min, 1h, 2h, 4h, 6h, 8h, 24h, 32h, 48h, 56h, 120h, 128h, 144h, 152h, 168h, 176h) and diluted to the total volume of 2.5 mL. The absorption peak at 426 nm was used to control the diffusion of curcumin. The experiments were carried out in triplicate.

ABTS free radical cation scavenging assay

An ABTS (2,2′-azino-bis(3-ethylbenzothiazoline-6-sulfonic acid)) free radical cation scavenging assay was performed as described in Fadda and colleagues [79]. ABTS radical cation (ABTS·+) was generated by the reaction between 7 mM ABTS water solution with 2.45 mM potassium persulfate solution in the dark at room temperature for 12–16 h. The ABTS·+ solution was diluted with water to obtain an absorbance of 0.80 a.u. at 734 nm. After that, 1×1 cm squares of each layer were cut and added to 3 mL of diluted ABTS·+ solution. The decrease in absorbance was determined at 734 nm with a Varian Cary 6000i Scan UV–visible spectrophotometer (Walnut Creek, California, USA) at different times. All measurements were carried out in triplicate, and the results were averaged to obtain a mean value. Radical scavenging activity (RSA) was expressed as the inhibition percentage of free radicals of the sample and calculated by using eq 3:

$$radical\ scavenging\ activity\ (\%) = \frac{A0 - A1}{A0} \times 100$$

where A0 is the absorbance value of the control radical cation solution and A1 is the absorbance value of the sample at different time points.

Biochemical oxygen demand

Biochemical oxygen demand (BOD) was performed to evaluate the biodegradability of the samples. Samples were cut into small pieces, and according to their composition, about 25 mg of material was added to 432 mL of seawater. Since BOD operates on the principle that microorganisms consume oxygen while decomposing organic substances present within the water, seawater collected from Old Harbor (Porto Antico) of Genoa was chosen as a liquid medium. Microbial consortia and saline nutrients required

for their establishment were already present, mimicking authentic natural circumstances. The experiment was conducted at room temperature to encourage microbial decomposition within amber glass bottles with a volume of 510 mL, hermetically closed with the OxiTop measuring heads. Sodium hydroxide tablets were added as a CO_2 scavenger to sequester carbon dioxide produced during biodegradation. Biotic consumption of the oxygen present in the free volume of the system was measured as a function of the decrease in pressure.

Samples were tested in triplicate. After 30 days, raw oxygen consumption data (mg O_2/L) were corrected by subtracting the mean values of the blanks obtained by measuring the seawater's oxygen consumption without any test material. After this subtraction, values were normalized on the mass of the individual samples and referred to 100 mg of material (mg O_2/100 mg material). BOD is calculated as the difference between the initial and final dissolved oxygen concentrations expressed as milligrams of oxygen per liter (mg/L) of water. Finally, the means of the triplicates were calculated and plotted vs time.

QUANTIFICATION AND STATISTICAL ANALYSIS

Molecular analysis

Quantification of chlorophyll a and c_2. Coral tissue was extracted from frozen fragments using a 1000 µL pipette tip connected to a benchtop air pressure valve via a rubber hose, delivering airflow in combination with 5 mL of ice-cold phosphate-buffered saline (PBS) [80]. The resulting tissue slurry was then homogenized and centrifuged at 3600g for 4 minutes. After discarding the supernatant, the pellet was incubated in 100% acetone for 24 hours at 4 °C in dark. Post-incubation, the sample underwent another centrifugation at 3600g for 4 minutes, and the supernatant was collected to measure Chl a and c2 concentrations. Fluorescence readings at 630, 663, and 750 nm were applied to dinoflagellate-specific equations [81] and normalized to the coral surface area.

The remaining coral skeletons, after tissue removal, were treated with a 10% bleach solution and allowed to dry for 48 hours. To determine the surface area of each fragment, the paraffin wax dipping method was used [82]. The weight change of the wax-coated skeletons was compared to a standard curve generated with clay cylinders of known surface area, enabling the calculation of the skeletal surface area for each fragment.

Symbiodiniaceae density. Samples previously fixed in 4% formalin were used to count Symbiodiniaceae cells from six independent hemocytometer (Improved Newbauer) counts under an optical microscope (Leica Company, France), as previously described [83]. Cell density was calculated by normalizing the surface area of respective fragments [84].

Oxidative stress analysis

Protein extraction. Coral fragments were ground using a pre-chilled mortar and pestle, then transferred to tubes and homogenized in 750 µL of lysis buffer (50 mM Tris-HCl, pH 7.4, 150 mM NaCl, 10% glycerol, 1% NP-40 detergent, 5 mM EDTA) containing 1 mM phenylmethylsulfonyl fluoride (PMSF; Sigma-Aldrich). An initial centrifugation at 3000 rpm for 5 minutes was carried out to separate the skeletal material. The resulting samples were subjected to a second centrifugation (14,000 rpm, 4 °C, 15 minutes), and the supernatant was collected and promptly frozen at –80 °C for future analysis. Protein concentration in each sample was determined using the Bradford assay, with bovine serum albumin (BSA) used to create the calibration curve.

Superoxide dismutase activity assay. Superoxide dismutase (SOD) activity was measured following the method of Vance and colleagues [85]. SOD activity is determined by its ability to compete with ferricytochrome c for superoxide radicals ($O_2^{\cdot-}$) generated by the xanthine/xanthine oxidase system, inhibiting the reduction of ferricytochrome c. The reaction mixture included the following reagents (Sigma-Aldrich): 0.01 mM ferricytochrome c, 0.1 mM EDTA, 0.01 mM xanthine, and 0.0061 U xanthine oxidase, prepared in a final volume of 1 mL. Various sample volumes were added to the reaction mixture to achieve 50% inhibition of the reaction rate. The reduction of ferricytochrome c was monitored spectrophotometrically at 550 nm and 25 °C using a Varian Cary 50 Scan Spectrophotometer (Agilent Technologies). Under these conditions, one unit of SOD activity was defined as the amount of enzyme required to inhibit the reduction of ferricytochrome c by 50%. Results are reported as units (U) of enzyme activity per milligram of protein.

Catalase activity assay. Catalase (CAT) activity was assessed using its peroxidation function, following the method described by Bergmeyer and Graßl [86]. The assay measured the enzyme-driven breakdown of hydrogen peroxide (H_2O_2). The reaction mixture,

prepared in a 1 mL cuvette, included 50 mM sodium phosphate buffer (pH 7.5) and 12 mM H_2O_2, to which varying sample volumes were added. The decrease in H_2O_2 concentration was tracked spectrophotometrically at 240 nm using a Varian Cary 50 Scan spectrophotometer (Agilent Technologies). Enzyme activity was expressed as units (U) per milligram of protein, where one unit (U) corresponds to the first-order rate constant (min^{-1}), as outlined in reference [87].

Glutathione S-transferase activity assay. GST activity was assessed by considering the reaction of the enzyme with the 1-Chloro-2,4-dinitrobenzene (CDNB) substrate, according to Hayes and Strange [88]. The reaction solution (containing 200 mM potassium phosphate buffer pH 6.5, 20 mM CDNB dissolved in 95% ethanol, and 20 mM reduced glutathione) was mixed in a 1 mL cuvette with different volumes of samples, and the formation of CDNB-oxidized glutathione conjugate was followed spectrophotometrically at 340 nm (Varian Cary 50 Scan spectrophotometer, Agilent Technologies). GST activity is expressed as units (U) of enzyme per mg of protein and is proportional to the increase in absorbance caused by conjugated product formation.

Glutathione reductase activity assay. The enzymatic assay of glutathione reductase (GR) was performed according to Wang and colleagues [89]. The activity of GR was evaluated through the spectrophotometric detection of the absorbance at 340 nm (Varian Cary 50 Scan spectrophotometer, Agilent Technologies) of NADPH oxidation to NADP+ reaction, which occurs in conjunction with the glutathione reduction, and is proportional to the decrease in absorbance over time. NADPH reaction was initially measured in the reaction mix (containing 0.1 M potassium phosphate buffer pH 7.6, 0.16 mM NADPH, 1 mg ml^{-1} BSA and 4.6 mM oxidized glutathione) and subsequently adding different volumes of the sample. GR activity was obtained from the difference of the two absorbance values. One unit of GR activity is defined as the oxidation of 1 nmol NADPH/min at 25°C. Results are expressed as units (U) of enzyme per mg of proteins.

Lipid peroxidation. Lipid peroxidation levels were evaluated by measuring malondialdehyde (MDA) concentrations using a commercially available assay kit (Bioxytech LPO-586, Oxis International, USA). This method relies on the reaction between MDA and the chromogenic reagent N-methyl-2-phenylindole at 45 °C. Coral apex samples (~1 g each) were pulverized using a pre-chilled mortar and pestle and then homogenized in 1 mL of 20 mM phosphate buffer (pH 7.4). To prevent oxidation during processing, 10 µL of 0.5 M butylated hydroxytoluene in acetonitrile was added to each 1 mL homogenate. The homogenates were centrifuged at 3,000 × g for 10 minutes at 4 °C, and the supernatant was collected for protein quantification using the Bradford method.

The assay was performed following the hydrochloric acid solvent procedure provided by the kit's manufacturer. The absorbance of the resulting blue product was measured at 586 nm, as described by Gérard-Monnier and coworkers (1998) [90]. Results are expressed as µmol of MDA per µg of protein.

Statistical analysis

Statistical analyses were performed using OriginPro software (OriginLab Corporation, Northampton, MA, USA). Data normality was verified using the Shapiro-Wilk test, and when assumptions were violated, appropriate transformations were applied. A one-way ANOVA test was applied to evaluate differences among experimental groups. When significant differences were detected, a Tukey post-hoc test was used to determine pairwise comparisons between the control and three-layered film system-treated samples. A p-value < 0.05 was considered statistically significant and highlighted by (*) in the graphs. Data are presented as arithmetic means with standard error, with n=3 for each biomarker analyzed. Moreover, effect sizes (η^2) were calculated to complement p-values and better describe the magnitude of treatment effects.